Quaternary Science Reviews 333 (2024) 108684

Contents lists available at ScienceDirect

Quaternary Science Reviews

journal homepage: www.elsevier.com/locate/quascirev

Invited Review

Speleothems in subglacial caves: An emerging archive of glacial climate history and mountain glacier dynamics

Christoph Spötl [a,*], Jonathan L. Baker [a], Vanessa Skiba [b,c], Alexandre Honiat [a], Jens Fohlmeister [d], Marc Luetscher [e], Martin Trüssel [f]

[a] Institute of Geology, University of Innsbruck, Innrain 52, 6020, Innsbruck, Austria
[b] Alfred Wegener Institute, Helmholtz Centre for Polar and Marine Research, Potsdam, Germany
[c] Potsdam Institute for Climate Impact Research, Member of the Leibniz Association, Potsdam, Germany
[d] German Federal Office for Radiation Protection (BfS), Köpenicker Allee 120, 10318, Berlin, Germany
[e] Swiss Institute for Speleology and Karst Studies, Serre 68, 2300, La Chaux-de-Fonds, Switzerland
[f] Foundation Naturerbe Karst und Höhlen Obwalden (NeKO), Alpnach, Switzerland

ARTICLE INFO

Handling editor: Dominik Fleitmann

ABSTRACT

Speleothems from cold high-elevation (and high-latitude) caves are sensitive paleoenvironmental archives, because they form close to the freezing point of water, and Alpine or Arctic soils – the source of carbon dioxide for carbonic-acid dissolution – are thin and experience a short vegetation period. Climatic cooling is therefore likely to disrupt the growth of these speleothems. However, growth hiatuses may paradoxically be overcome when atmospheric cooling leads to lowering of the equilibrium-line altitude and expansion of temperate glaciers over the karst system, which prevents the latter from freezing. Caves in mountain regions of the mid to high latitudes had a much higher chance of being covered by glaciers during cold climatic periods than caves at lower elevations, which were often in the permafrost zone. These periods without frost in caves covered by temperate glacier ice can be recorded by so-called subglacial speleothems if the host rock contains disseminated pyrite. Widely present in impure limestones, dolostones, and marbles, oxidation of this sulfide mineral gives rise to sulfuric-acid dissolution of the host rock, replacing the carbonic-acid dissolution that operates during warm climate periods.

This review summarizes the research history of subglacial speleothems, beginning with seminal studies of Castleguard Cave, which extends beneath the Columbia Icefield in Western Canada. Subsequent work on a number of caves in the Eastern and Western Alps in Europe has shown that speleothems from such subglacial environments are widespread and provide unprecedented opportunities to obtain records of environmental change covering the long glacial periods. However, the proxy system behavior of these settings has yet to be fully developed. We therefore propose a suite of diagnostic criteria, some untested, by which to identify and interpret subglacial speleothems, with recommendations for future research. The combination of high $\delta^{13}C$ (at or above host rock values) and low $\delta^{18}O$ provide a robust first-order proxy for subglacial environments, while trace-element and sulfate stable-isotope ($\delta^{34}S$ and $\delta^{18}O$) data can elucidate the dissolution pathway and redox conditions resulting from ice cover. When studies of subglacial speleothems are combined with conventional warm-climate speleothems controlled by soil dynamics, as well as locally present cryogenic cave carbonates (an indicator of the presence of paleo-cave ice accumulations), the possibility of exploiting the full paleoclimate potential of Alpine and Arctic caves on glacial-interglacial timescales opens up.

1. Introduction

Speleothems, mineral deposits formed in caves, are commonly composed of calcium carbonates such as calcite. They form by degassing of carbon dioxide from cave waters, which originate as meteoric water and derive their dissolved solids by dissolution of limestone or dolomite (see summary by Fairchild and Baker, 2012). Stalactites, stalagmites, and flowstones are the most common types of speleothems. They form in

* Corresponding author.
E-mail address: christoph.spoetl@uibk.ac.at (C. Spötl).

https://doi.org/10.1016/j.quascirev.2024.108684
Received 23 March 2024; Accepted 22 April 2024
Available online 3 May 2024

vadose cave settings fed by drip water. Other types of speleothems include mammillary calcite, which forms subaqueously (e.g., Hill and Forti, 1997; Kolesar and Riggs, 2004), and cryogenic cave carbonates, whose origin is related to freezing processes in ice-bearing caves (Žák et al., 2018).

Speleothems serve as archives of climatic and environmental history, as their formation is ultimately controlled by meteoric precipitation, and the cave microclimate – apart from some exceptions – reflects the mean air temperature outside the cave. As a consequence, cold and dry climate episodes are often recorded in speleothems by hiatuses, and speleothem deposition in mid- and to high-latitude caves is biased toward interglacials. Well-studied sites showing growth predominantly during such warm and humid climate periods include Villars Cave in France (Genty et al., 2005), Lancaster Hole in England (Baker et al., 1996), Crag Cave in Ireland (Fankhauser et al., 2016) and caves in Siberia (Vaks et al., 2013). The same applies to arid regions, e.g. in the subtropics, which experienced intermittent wetter conditions in the past. Examples include Rössing Cave in the Namib Desert (Geyh and Heine, 2014), Hoti Cave in Oman (Burns et al., 1998), Mukalla Cave in Yemen (Nicholson et al., 2020) and Kesang Cave in western China (Cheng et al., 2012).

Speleothems also provide valuable insights into soil and vegetation conditions given that karst dissolution is driven by carbonic acid derived from the dissolution of soil carbon dioxide (carbonic-acid dissolution; hereafter CAD). The presence of a vegetated catchment with a well-developed soil zone is therefore key for effective karst dissolution and subsequent re-precipitation of carbonates in caves beneath. As a consequence, caves located in regions with dense vegetation and well-developed soil are typically characterized by abundant speleothem decoration and comparably high rates of carbonate deposition. In contrast, caves whose catchments are barren, commonly show no or only limited (and very slow) speleothem growth (e.g., Borsato et al., 2016). The lack of significant vegetation and soil development in these settings can be due to an arid climate and/or low temperatures, e.g., the presence of permafrost. Finally, the cave catchment can become glaciated, which terminates pedogenetic processes and will likely result in the erosion of any pre-existing soil. Paradoxically, this extreme scenario can locally open a new "window" for speleothem deposition. This class of speleothems, referred to as subglacial speleothems,[1] is an emerging field in speleothem science with great potential for paleoclimate studies of Pleistocene cold periods and constitutes the motivation for this review article.

2. Subglacial speleothems: the basic concept

The advance of glaciers across the catchment of caves will affect the karst beneath in at least three fundamental ways: (a) Elimination of vegetation and erosion of soil, essentially stopping the influx of soil-derived carbon into the karst system. As a consequence, rates of carbonic-acid driven karst dissolution will be greatly diminished, and "normal" speleothem deposition will come to a halt. (b) Fundamental change of the discharge regime from direct infiltration of rain- and/or snowmelt-water through the soil before glaciation to the influx of snow- and ice-melt water at the base of a glacier (Fig. 1). Previous studies have shown that the drainage of subglacial meltwaters commonly utilizes karst conduits, resulting in erosion (Lauritzen and Skoglund, 2022) and/or deposition of clastic sediments (e.g., Jaillet et al., 2023). Deposition of speleothems is impossible in such conduits occupied by high-energetic meltwater streams and/or prone to flooding. (c) The thermal regime of the karst rock will change depending on the starting conditions (e.g., the presence of permafrost) and the type of glacier. A warm-based glacier will maintain the rock beneath at non-freezing temperatures, while cold-based ice will result in a permanently frozen substrate (Fig. 1).

The first boundary condition that needs to be met in order to open a "window" for speleothems to potentially form underneath a glaciated landscape is therefore that the ice must be temperate, i.e. at or slightly above the pressure melting point of water at the base of the glacier (Hodson et al., 2008). Such warm-based glaciers are the norm in today's glaciated regions outside of Antarctica. Also many of the much larger glaciers that existed during glacial periods were warm-based as shown by the presence of U-shaped valleys, fjords, roches moutonnées, and many other erosional features in formerly and/or presently glaciated mountain ranges. In contrast, in mid-latitude mountain ranges, cold-based ice can be found today only at high altitudes (e.g., on some high peaks in the European Alps – Haeberli et al., 2004; Fischer et al., 2022). The net effect of the presence of warm-based ice is to isolate the underlying bedrock thermally from winter-air cooling, while heat influxes from surface meltwater infiltration and geothermal conduction prevent permafrost formation.

A second requirement is that a given cave passage where speleothems form is not invaded by meltwater. Such sheltered passages are locally present in mountain caves as shown by many studies documenting stalagmites and flowstones that "survived" multiple glaciations (Häuselmann et al., 2008; Columbu et al., 2018; Bajo et al., 2020; Szczygieł et al., 2020). Such protected cave passages may be less widespread in karst regions that were buried beneath large ice sheets during glacial advances. Studies of Norwegian caves located near the Polar Circle, however, have shown that even some of these sites, which were repeatedly covered by the Scandinavian Ice Sheet, preserve speleothems spanning up to half a million years (e.g., Lauritzen and Skoglund, 2022).

Finally, even if a warm-based glacier is present (preventing the cave underneath to turn into an ice cave) and the cave galleries are protected from meltwater streams, no speleothems would form because of minimal karst dissolution in the absence of soil carbon dioxide. The third and final requirement therefore is that the soil-driven karst process is replaced by a different dissolution reaction that does not involve carbonic acid. This is sulfuric acid generated by the decomposition (oxidation) of sulfide minerals, commonly pyrite. Such Fe-sulfides are widespread at low abundances in impure carbonate rocks and more so in marls and shales, e.g., in contact-karst settings. If such lithologies are present, typically characterized by medium to dark-gray color reflecting elevated contents of organic carbon, they will release sulfuric acid to the seepage water, which readily dissolves carbonate rocks (sulfuric-acid dissolution; hereafter SAD). CO_2 degassing of such waters upon entering caves will result in supersaturation with respect to calcite and the precipitation of speleothem carbonates.

3. Discovery of subglacial speleothems: Castleguard Cave

The birthplace of the concept of speleothem deposition in caves underneath a glacier is Castleguard Cave, located in the northwest corner of Banff National Park in the Rocky Mountains of Alberta, Canada (Fig. 2). This 21.3 km long cave (as of 2020) – the longest in Canada – opens at an altitude of 1998 m a.s.l. and terminates underneath the Columbia Icefield, the largest ice field in North America's Rocky Mountains, which stretches along the Continental Divide on the border between Alberta and British Columbia. Slightly more than half of this elongated cave is outside the icefield, and the surface above ranges from forested at lower elevations to barren rock and moraines in the permafrost zone at high elevations. The inner part of the cave traverses underneath the southeastern margin of the Columbia Icefield, and several galleries terminate with permanent ice plugs (Fig. 3). These innermost parts of the cave are overlain by about 300 m of ice.

Pioneering research led by Derek Ford and his team at McMaster University, Hamilton, Ontario, in the 1970s and 1980s has shown that despite its subglacial setting, the inner part of Castleguard Cave hosts speleothems. These formations are mostly calcitic in composition, but

[1] Not to be confused with subglacial carbonate crusts formed at the base of temperate glaciers (e.g., Hallet, 1976; Refsnider et al., 2012; Lipar et al., 2021).

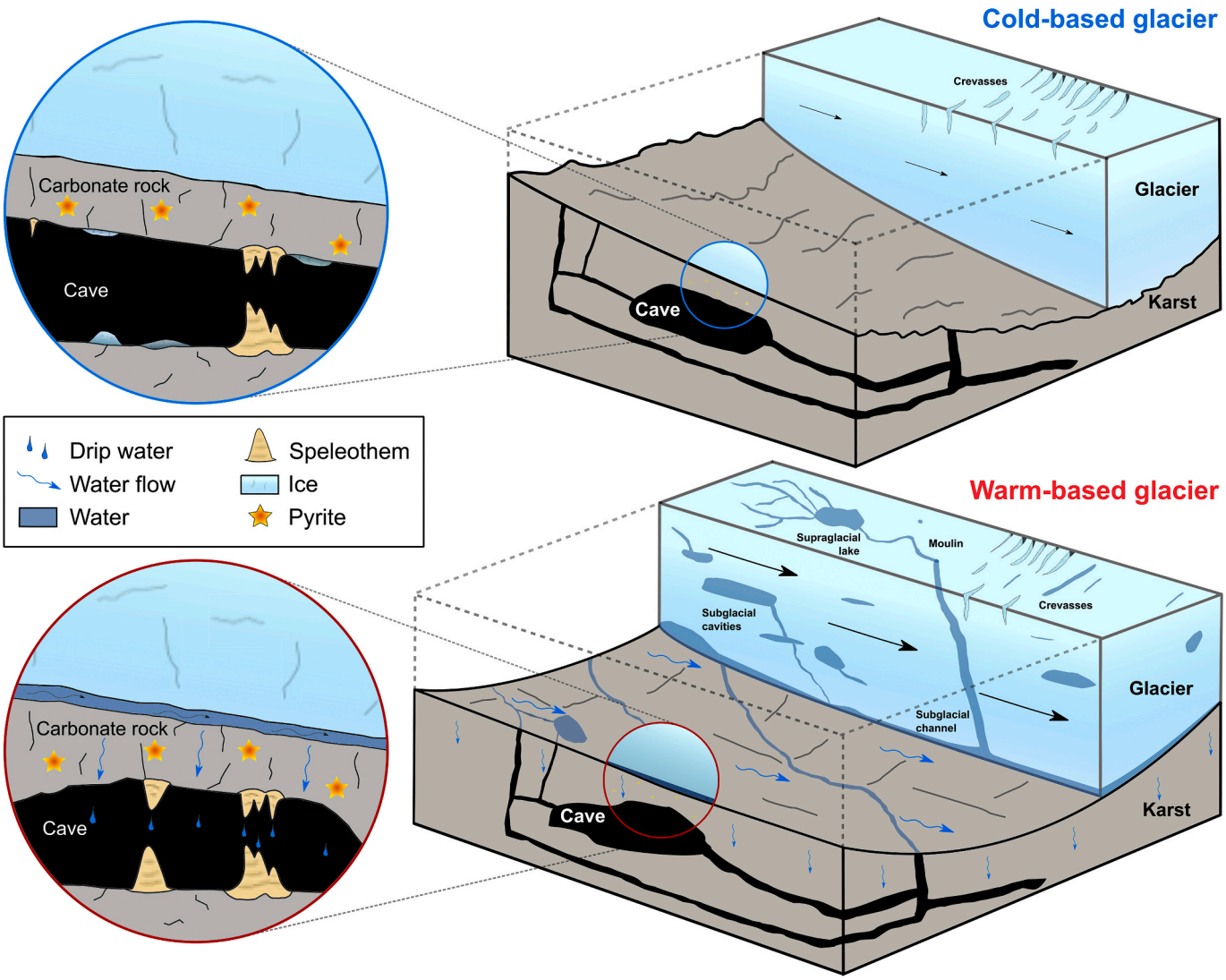

Fig. 1. Schematic overview of the two types of subglacial cave settings. Caves in rock overlain by a cold-based glacier contain perennial ice but no speleothems (with the exception of cryogenic ones). In contrast, karst rock underneath temperate (i.e. warm) ice contains liquid water, and in the presence of sulfide minerals such as pyrite, karst dissolution and speleothem growth can be sustained.

other minerals such as aragonite and gypsum have also been found (Harmon et al., 1983). Calcite speleothems comprise soda straws, stalactites, flowstones, and stalagmites. Several galleries of Castleguard Cave have recent and partly active speleothem formations, notably soda straws, stalactites, helictites and some stalagmites (Fig. 4).

In an attempt to constrain the age distribution of these speleothems, broken soda straws (partly helictites) and stalactites from four locations (three of them located underneath the glacier) were sampled. ^{230}Th-ages ranged from 2.6 ± 0.2 ka to 11.1 ± 0.7 ka BP (Gascoyne and Nelson, 1983). These analyses were performed by alpha spectrometry requiring large sample sizes, a technique that was gradually replaced by mass spectrometric techniques in the early 1990s. The data show no trend towards younger ages with increasing distance from the cave entrance to its interior as would be expected if the ice cover had retreated during the Holocene (Gascoyne, 1992). Conventional ^{14}C ages obtained on the same samples (again requiring large sample weights of about 30 g) were systematically older than their corresponding ^{230}Th-ages by about 4–10 ka and ranged from 4.1 ± 0.4 to 18.2 ± 0.3 ka BP (Gascoyne and Nelson, 1983). These findings are partly supported by a single ^{14}C analysis of dissolved inorganic carbon of seepage water from a site located underneath the very margin of the icefield which yielded a conventional ^{14}C age of 4.1 ± 0.4 ka BP (equivalent to 59.5 ± 3 % modern carbon; Gascoyne and Nelson, 1983) (see Fig. 4).

An additional 22 samples obtained from 16 other speleothems in Castleguard Cave (including massive and heavily corroded formations) yielded ages ranging from 1 ± 0.5 ka to > 350 ka BP (Harmon et al., 1977; Gascoyne et al., 1983), the latter representing the upper limit of the alpha-decay counting technique. Given the inherently large uncertainties of these measurements it is difficult to compare growth intervals to known paleoclimate periods, but the existing data suggest growth during Marine Isotope Stages (MIS) 1, 3, 5.3, 5.5 and 9, and possible growth during MIS 6, 7.5 and 8 (Gascoyne et al., 1983). These chronological data have been interpreted as evidence that the Columbia Icefield was present and temperate at its base during the time intervals represented by growth of these speleothems (Ford et al., 1976). This interpretation was later partly questioned based on a radiocarbon date of a sample recovered from the uppermost end of the cave, described as "red squirrel midden" (8.48 ± 0.11 ^{14}C ka BP, ca. 9.7–9.2 cal ka BP). If this animal was indeed introduced into the cave via the currently ice-blocked headward passage (Dessert Glace), then the icefield may have either receded just enough to expose that particular ice plug to allow the animal access or disappeared almost entirely during the early Holocene (Ford and Smart, 2017; Luckman et al., 2020). Indeed, glaciers throughout western Canada were generally smaller between about 11

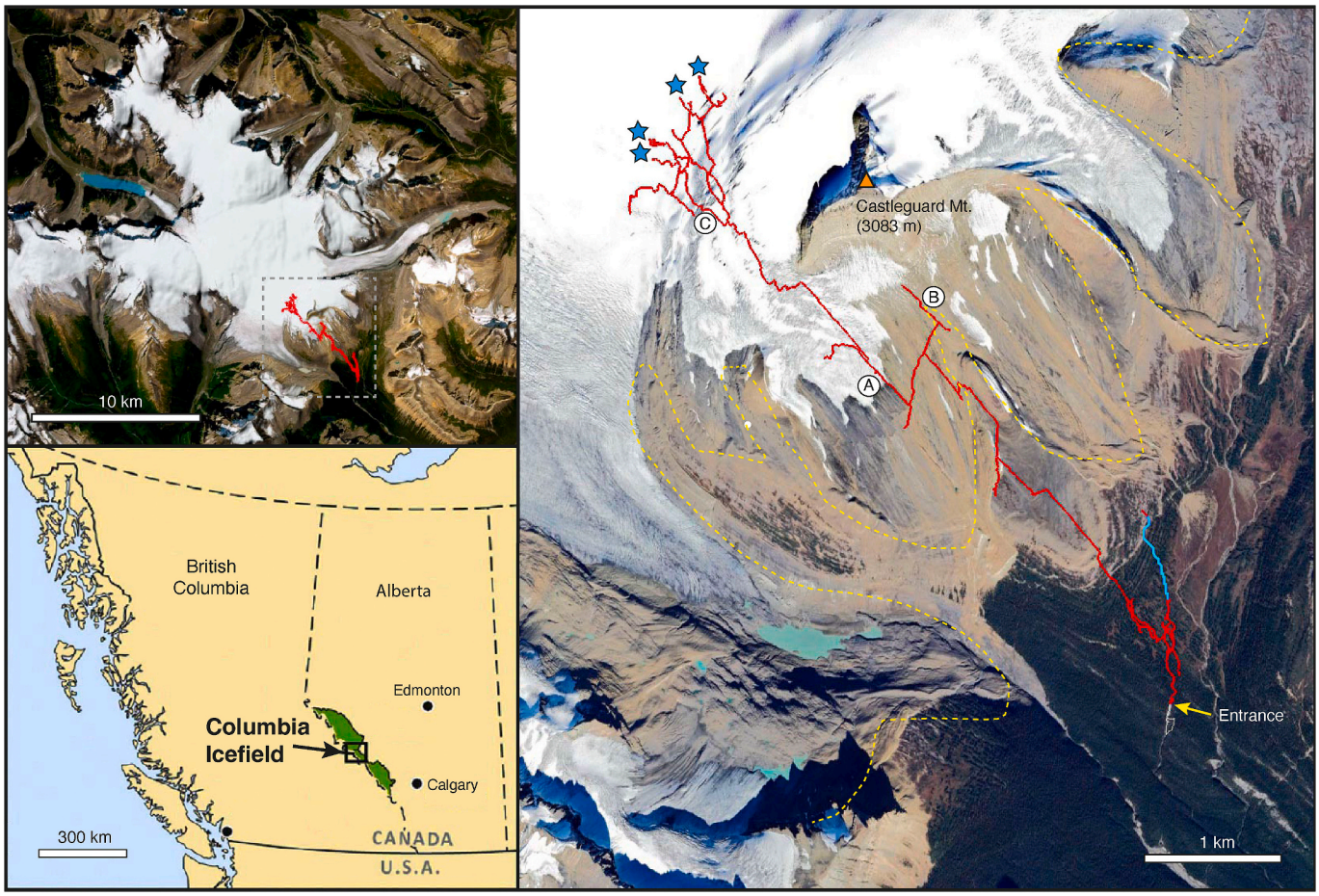

Fig. 2. Geographic setting of Castleguard Cave. Top left: Satellite image of the Columbia Icefield showing the trace of the cave in red (vadose parts) and light blue (phreatic part). The dashed rectangle marks the position of the enlarged view on the right showing the plan view of the cave extending from the entrance in the southeast underneath the margin of the icefield, ending in several ice plugs (blue stars; GoogleEarth). The 1919 AD extent of the nearby glaciers is shown by the dashed yellow line (after Tennant and Menounos, 2013). Letters A-C refer to locations in the cave where images shown in Fig. 3 were taken.

and 7 ka BP than during the second half of the Holocene (e.g., Menounos et al., 2009). This has obvious consequences for the question of whether the deposition of speleothems took place in a subglacial environment. Today, only the inner part of Castleguard Cave beyond the gallery called Holes in the Floor (letter A in Fig. 2) is a subglacial position. When the first glacier survey of the Columbia Icefield was made in 1919 (Tennant and Menounos, 2013), the glacially covered part extended further to the southeast (dashed yellow line in Fig. 2), and during the Little Ice Age this extent was even slightly larger judging from the fresh appearance of moraine ridges. The last time the entire cave system was likely covered by ice was towards the end of the Younger Dryas, following major ice loss of the Cordilleran Ice Sheet at the onset of Bølling (ca. 14.7 ka BP; Menounos et al., 2017).

A study of drip water associated with recent speleothems showed that these waters were supersaturated with respect to calcite, while flows of water on cave walls showing corrosion features were undersaturated (Atkinson, 1983). Several processes were considered in order to explain the presence of supersaturated seepage waters (and associated speleothem deposition) in the absence of a soil source: (a) Degassing of carbon dioxide and concomitant slight supersaturation and precipitation of calcite due to a warming of the waters upon entering the cave, a model that was put forward by Dreybrodt (1982) based on chemical kinetic considerations. The interior of Castleguard Cave is about 3°C and indeed warmer than the outside, an effect that was attributed to weak geothermal heating (Ford et al., 1976). This slight warming of the seepage waters, however, was deemed insufficient to account for speleothem deposition (Atkinson, 1983). (b) Evaporation of seepage waters was also found to play only a minor part in the precipitation of calcite speleothems, although this process is of importance for the occurrence of hydrated carbonate (e.g., hydromagnesite) and sulfate minerals (e.g., mirabilite), particularly in the innermost parts of the cave (Atkinson, 1983; Harmon et al., 1983). (c) Dissolution of Ca-sulfate minerals in rocks above the cave. Adding a second Ca source in addition to the dissolution of calcite and dolomite would increase saturation with respect to calcite (common-ion effect). Ca-sulfate evaporites, however, have only been observed as rare vein fillings in one of the limestone formations and were therefore not regarded as relevant for speleothem formation (Atkinson, 1983). (d) The main process that was identified to cause speleothem deposition in Castleguard Cave is the oxidation of pyrite. Pyrite is present in small amounts in all limestones and interbedded dolomites above the cave, as shown by rusty weathering spots. In some rock units, macroscopic pyrite crystals and small nodules (concretions) were observed (Atkinson, 1983). The reaction of iron sulfides with seepage water derived from melting of snow and ice releases sulfuric acid, which dissolves calcite and dolomite in the host rock in the absence of carbonic acid. This model is consistent with the elevated sulfate concentration in the seepage waters (reaching up to 223 mg/l) and with stable C isotope data of Holocene speleothems which show $\delta^{13}C$ values between −1.5‰ and +1.6‰, i.e. indicating no pedogenic C input (Gascoyne and Nelson, 1983; unfortunately, there is no systematic $\delta^{13}C$ study of Pleistocene speleothems from this cave). A subsequent study examined gypsum speleothems from Castleguard Cave using stable isotope techniques. Gypsum $\delta^{34}S$ values cluster in the +14 to +16‰ range, bracketing the values of pyrite in the cave rocks (Yonge

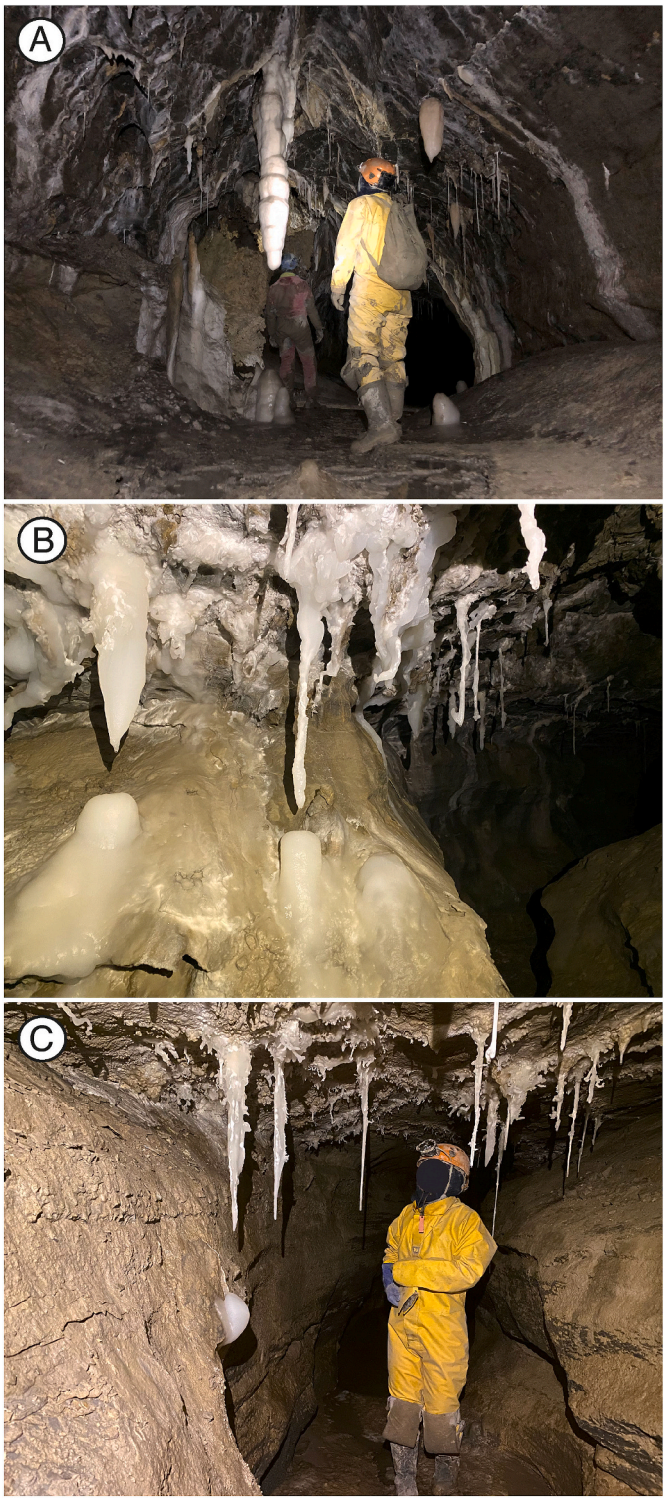

Fig. 3. Speleothems in Castleguard Cave (locations shown on the cave map in Fig. 2). A: Gallery showing abundant stalactites, soda straws and stalagmites ("Holes in the Floor"). B: Active stalagmites, stalactites, helictites and flowstones. Width of image ca. 1.5 m ("The Next Scene"). C: Stalactites, helictites and a small stalagmite ("Munchkin Peon Trail"). Image A courtesy of Jeremy Bruns and Images B and C courtesy of Christian Stenner.

and Krouse, 1987; one gypsum sample yielded a much higher value suggesting dissolution of marine-derived anhydrite).

The observation that Castleguard speleothems apparently formed from seepage waters lacking a pedogenic C source led Atkinson (1983) to speculate that these findings may have "important consequences in the area of paleoclimatology" because "the minimum climatic requirement for speleothems to grow at least slowly is a supply of water. The only circumstances in which water is likely to be totally cut off is where the cave temperature is below 0 °C or where a warm cave lies beneath truly continuous permafrozen ground" (p. 535). Interestingly, Atkinson's prediction that speleothem formation underneath a temperate glacier should be more widespread in particular during colder times of the Pleistocene when glaciers were more abundant did not spark new discoveries in the following years. This was probably partly due to the fact that few researchers worked in Alpine caves, and research on speleothems only became a fully accepted part of terrestrial paleoclimate science with the advent of accurate and precise dating techniques based on mass spectrometry in the late 1980s (e.g., Edwards et al., 1987) and subsequent technical improvements. The pioneering phase of research on Castleguard Cave ended in the 1980s, and apart from cave exploration (e.g., Horne, 2017; Harris et al., 2021) and monitoring of seasonal ice buildup and flooding near the cave entrance (Horne et al., 2019), no new major geoscientific research has been carried out since then. This is largely due to the logistic challenges as the cave can only be safely accessed in winter and requires camps, and has stringent access requirements, even for research.

With regard to the wider Canadian Rocky Mountains, there are indications that Castleguard may not be the only subglacial cave hosting speleothems. Unfortunately, little published documentation exists about caves in this vast and remote region. For example, Steaming Shoe is a 210 m long cave located outside the northwestern boundary of Banff National Park. It opens beneath the Icefall Brook and is overlain by the Lyell Glacier. The cave is reported to be decorated with some stalactites and soda straws (Rollins, 2004). Other caves currently (or until recently) situated in a subglacial setting have been reported — e.g., in the Hawk Creek karst, Moon River karst, on the Dezaiko Plateau, and on Mt. Robson —although it remains unknown whether they also contain speleothems (Rollins, 2004).

4. Lessons from the European Alps: caves in the Eastern Alps

The wave of research on Castleguard Cave was followed by a pause in research activity on the subject of subglacial speleothem deposition. In the 1980s and early 1990s, modern speleothem science was still in its infancy and there were only a few groups worldwide dedicated to this topic. Their research was targeted mostly towards caves outside formerly glaciated areas such as the subtropics (e.g., Winograd et al., 1992; Wang et al., 2001). Speleothem-related research that was carried out at or near areas of large glacier extent during glacial periods suggested that speleothem deposition in the mid-to high northern latitudes was biased towards warm climates, i.e., interglacials and prominent interstadials (e.g., Lauritzen, 1995; Baker et al., 1996; Berstad et al., 2002; Genty et al., 2003).

At the turn of the century, the Innsbruck Quaternary Research Group began its work in the European Alps, more precisely the Eastern Alps of Austria. This research involved ^{230}Th-dating using thermal ionization mass spectrometry in collaboration with the University of Heidelberg, Germany. Up to this point, limited speleothem research had been carried out in Alpine caves of Austria (Seemann et al., 1997), Switzerland (Wildberger et al., 1991), Italy (Frisia et al., 1993), and France (Maire, 1990), and none had involved ^{230}Th-dating using mass spectrometry. Despite their high elevation and the associated low temperatures, speleothems were found in several Alpine caves in Austria (Figs. 5a and 6). Two neighboring caves on the crest of the Eastern Alps became the focus of this activity, Spannagel Cave (12 km in length) and Kleegruben Cave (200 m long). Their (upper) entrances are located at 2524 and 2182 m a.s.l., respectively. Today, the area above both caves is ice-free and interspersed with sparse Alpine mats and barren rock, and the tree line is located close to 2000 m a.s.l. In the 1930s, however, the western part of Spannagel Cave was still covered by the tongue of the Hintertux glacier,

Fig. 4. One of the ice plugs in the innermost part of Castleguard Cave providing a water- and air-tight seal of a paleophreatic passage. This point is overlain by approximately 10 m of rock and some 230 m of ice of the Columbia Icefield. Left image taken in 1974 (photograph by Anthony Waltham), right image taken in 2020 (photograph by Jeremy Bruns). Note minimal ice ablation in 46 years.

and during the height of the Little Ice Age (16th to 19th century), up to two thirds of this cave was buried under ice (Spötl and Mangini, 2010). Kleegruben Cave was not covered by ice during the Little Ice Age, but during the Younger Dryas (Zasadni, 2009).

Investigations revealed formations in several galleries of Spannagel Cave, including those in the western part that was overlain by ice as recent as the early 20th century. Growth occurred during MIS 1, 3, 5.1, 5.5., 7.1 to 7.5, 8, 10, 14 and possibly 15 (Holzkämper et al., 2005; Spötl and Mangini, 2007, Spötl et al., 2007, 2008; Cliff et al., 2010; Wendt et al., 2021 – Fig. 7). A series of sites show active drips, and the drip water is variably supersaturated with respect to calcite. Kleegruben Cave is smaller and shows only few active drips. Dating of an inactive stalagmite from Kleegruben Cave revealed a continuous record of calcite deposition during MIS 3 (Spötl and Mangini, 2002). Later validated by a second stalagmite that spans the same time interval (Spötl et al., 2006), this record demonstrated uninterrupted calcite deposition across stadial-interstadial climate swings, including a Heinrich event.

Using $\delta^{13}C$ as an indicator of soil-derived C input, only MIS 1 and 5.5 were warm enough for the catchment above the two caves to become fully deglaciated and for vegetation and soil to develop (there are currently no speleothem data on MIS 11 from these two caves). There is some indication that the glacier above Kleegruben Cave had retreated during MIS 3, given that $\delta^{13}C$ data corrected for prior calcite precipitation (PCP) tend to fall below minimum host-rock values (Skiba et al., 2023b), but this question remains under investigation. It follows that during the other intervals represented by dated speleothems, the Hintertux glacier covered (most of) the caves and remained warm-based. The only times when this glacier may have become cold-based was during MIS 2 and 6; however, this inference is made indirectly from the paucity of ^{230}Th-ages (from a database of about 350 ages) within the last two glacial maxima (Fig. 7).

The source of the acidity required for karst dissolution in the absence of soil gas is related to the tectonic setting of these caves. They are confined to a ca. 20 m-thick layer of marble that rests conformably on paragneiss and is overthrusted by older orthogneiss (contact karst). Both the overthrusted gneiss and the marble, a medium gray and partly graphitic calcite marble with minor dolomite intercalations, contain sulfide minerals (pyrite, but locally also Cu-bearing sulfides). The oxidation of these sulfides is not only indicated by the occurrence of rusty coatings, but also by elevated sulfate concentrations in the drip waters and locally abundant gypsum on cave walls and ceilings. The S isotopic composition of gypsum supports an origin from sulfide oxidation (Spötl et al., 2004).

Spannagel Cave and Kleegruben Cave therefore share several similarities with Castleguard Cave, with the main difference being that the two Austrian caves are no longer overlain by a glacier. This lack of modern cover precludes actualistic studies of such a subglacial environment using monitoring techniques. Thanks to the ^{230}Th-chronologies (and the high to very high U content of the speleothems), samples from these caves opened the door to obtain climate records from such high-elevation sites covering not only interglacials such as the Holocene (Mangini et al., 2005, 2007; Fohlmeister et al., 2013) and the Eemian (Holzkämper et al., 2004; Spötl et al., 2007), but also parts of the much longer glacial periods of the Middle to Upper Pleistocene.

5. Lessons from the European Alps: caves in the Western Alps

Research on subglacially formed speleothems was subsequently expanded to caves in the Western Alps (Fig. 5a). These mountains are on average higher than the Eastern Alps and closer to the oceanic moisture sources, hence hosting the largest glaciers in the European Alps. In a search for sites directly associated with modern glaciers, Milchbach Cave was chosen. This multi-level system opens at 1840 m a.s.l. and developed on the left flank of the Upper Grindelwald Glacier, whose fluctuations are well documented for the past 450 years. Milchbach Cave hosts active speleothems including stalactites, stalagmites, flowstones and moonmilk. Four inactive stalagmites spanning 9.2 to 2.0 ka BP were examined in detail. They showed consistent petrographic and stable isotopic changes, which were attributed to abrupt changes in the cave environment as a result of the closing and opening of cave entrances due to the growth and retreat of the adjacent glacier (Luetscher et al., 2011). Speleothem growth during intervals of glacier coverage was at least in part related to the oxidation of pyrite present in the medium gray limestone, as shown by elevated sulfate concentrations in the drip waters and the presence of gypsum on the walls of the upper cave parts. Speleothem $\delta^{13}C$ values range between −3 and +1‰ and overlap with the values of the host limestone, suggesting only a small pedogenic C component during times of small glacier extent (Luetscher et al., 2011; even today the surface above the cave is largely barren rock).

A study that received wide attention reported stalagmite growth in the Sieben Hengste-Hohgant System (7H Cave for short hereafter) located also in Switzerland (Fig. 5a; Luetscher et al., 2015). This cave is an extensive network of about 171 km (as per 2023), 1.3 km of vertical extent and showing multiple entrances. Two stalagmites, found in-situ at 1540 m a.s.l., some 215 m below the inclined karst plateau, record calcite deposition between 30.0 and 14.7 ka BP (Figs. 8 and 9). This

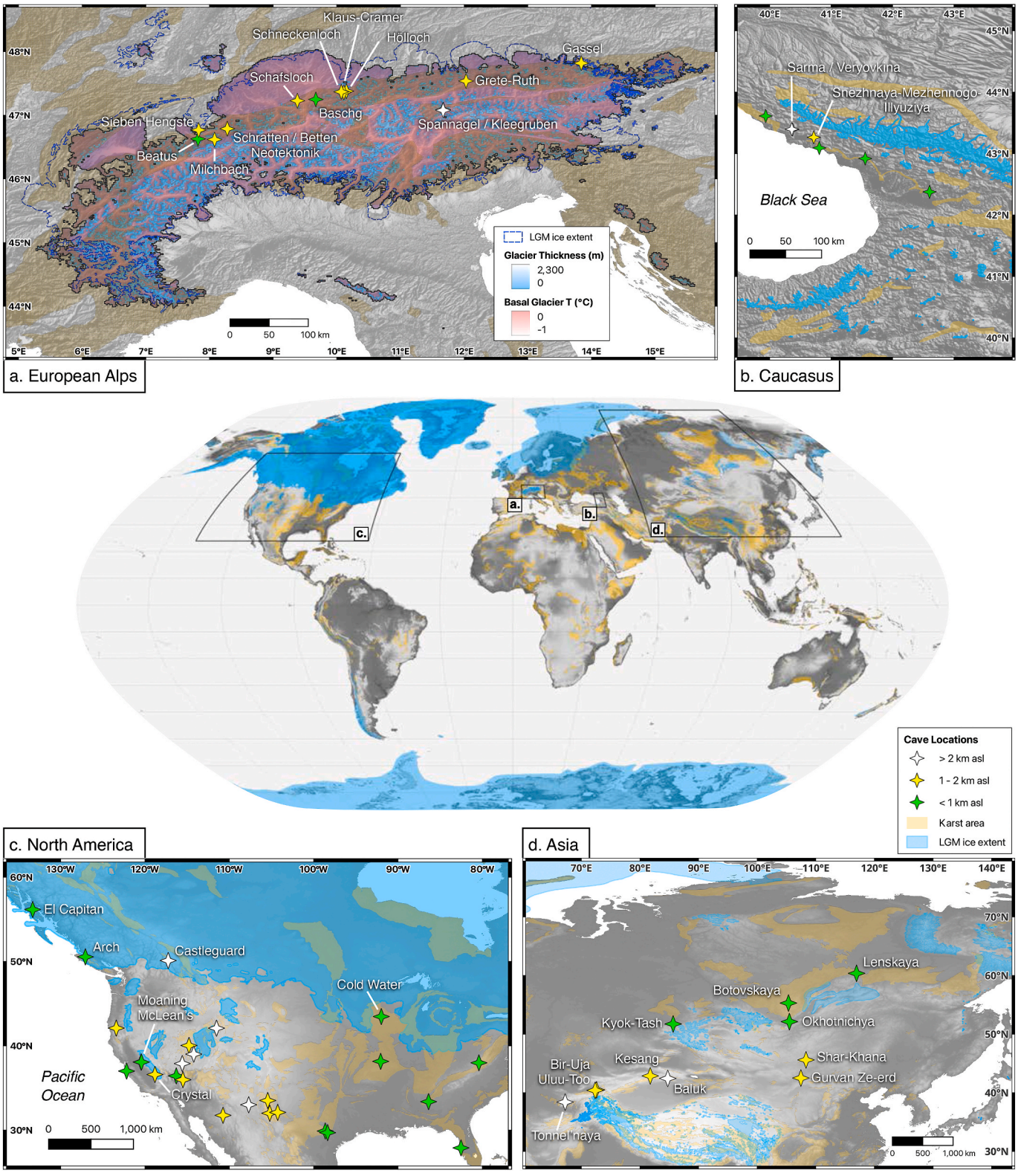

Fig. 5. Global and regional maps of karst and glacial ice extents. Center: World map shows global extent of karst terrain (yellow; Chen et al., 2017) and mapped limits of ice sheets and Alpine glaciers during the Last Glacial Maximum (blue; Ehlers et al., 2011). (a) Map showing cave sites in the European Alps that have been investigated for subglacial speleothems and fall within the empirical limit of LGM glaciers (dashed blue outline). Overlain is the model-reconstructed LGM ice margin (black outline), thickness (light blue), and the areal extent of warm-based glaciers (red) from Jouvet et al. (2023). (b) Map showing sampled cave sites in the Caucasus in relation to the LGM ice extent. Cave systems potentially within previous ice limits, based on altitude, are labelled. (c) Map showing North American cave sites from the SISALv2 database (Comas-Bru et al., 2020). Sites within or proximal to the LGM ice margin are labelled. (d) Map showing cave sites in northern Asia with published speleothem records or age data. Shaded relief for all maps is given by ETOPO1 (Amante and Eakins, 2009). Cave sites are denoted by stars, whose color-coded elevation corresponds to that of the cave entrance, as reported by the original publications.

Fig. 6. Holocene and partly active speleothems in Spannagel Cave (Märchenwelt). This part of the cave was in a subglacial position as recent as about 90 years ago. Image by Robbie Shone.

result was highly surprising, as their growth history brackets the Last Glacial Maximum (LGM, MIS 2) in the Alps, an extreme climate epoch that had not been captured by any speleothem from an Alpine cave and even outside the Alps is very poorly recorded by speleothems in European caves. The two stalagmites (and at least two more unpublished samples by M. Luetscher; Fig. 9) demonstrated for the first time that even during glacial maxima, at least some mountain caves in the Alps were warm enough to allow seepage water to exist for thousands of years and karst processes to operate. These special conditions were attributed to a combination of pyrite oxidation and the presence of a small temperate ice cap on the karst plateau (Luetscher et al., 2015). The lack of soil-derived C is supported by speleothem $\delta^{13}C$ values mostly between +3 and +6‰. These elevated values reflect the isotopic composition of the local Cretaceous host rock (mostly +2 to +3‰; Bonvallet, 2015), likely partly influenced by prior calcite precipitation. The O isotope records of the two stalagmites show a high degree of similarity and provided the first well-dated terrestrial proxy record for the LGM in Europe. The data show not only evidence of two short-lived interstadials previously known from ice cores in Greenland but also a marked depression in $\delta^{18}O$ between 26.5 and 23.5 ka BP (Luetscher et al., 2015). This interval of highly depleted $\delta^{18}O$ values, interpreted as a major southward shift of the storm tracks transporting Mediterranean moisture to and across the Alps, occurred during the time when Alpine glaciers reached their largest ice extent (Monegato et al., 2017). During these millennia, 7H Cave was bordering a major ice stream at least 1 km thick, which exported ice from the high mountains south and southeast of the site onto the Alpine foreland. Finally, the end of stalagmite growth at 14.7 ka BP associated with a sharp rise in $\delta^{18}O$ occurred precisely at the onset the Bølling interstadial and likely recorded the demise of the local glacier cover and associated changes in the local karst hydrological regime.

In a recent study focusing on the last interglacial at 7H Cave, Luetscher et al. (2021) reported rapid speleothem deposition since the end of the penultimate glacial. The stalagmite started growing 133.5 ka ago, encompassing Heinrich stadial 11. Similar to the LGM, the presence of a local ice/firn cover is supported by elevated $\delta^{13}C$ values between +4 and + 6‰, which decrease dramatically at the onset of MIS 5e (~130 ka BP).

An independent study reported data from a stalagmite retrieved from Schafsloch, a small cave located slightly higher than 7H cave (1890 m a.s.l.) in eastern Switzerland (Fig. 5a; Häuselmann et al., 2015). This speleothem began growing at 137.4 ± 1.4 ka BP, i.e. at the end of the penultimate glacial (which in the Alps was characterized by an ice stream network even larger than during MIS 2; Schlüchter et al., 2021) and several millennia prior to the onset of the Eemian (ca. 129.0 ka BP; Drysdale et al., 2005; Cheng et al., 2009). Similarly, $\delta^{13}C$ values of +6.5‰ indicate the absence of a soil signal during this time. The authors attributed this initial growth phase to an early warming event during Termination II, which led the local glacier above Schafsloch to switch from cold-to warm-based (Häuselmann et al., 2015). The Cretaceous limestone in which Schafsloch formed contains pyrite, thus explaining karst dissolution in the absence of soil. Interestingly, the stalagmite stopped growing between 133.1 ± 0.7 ka BP and re-commenced at 131.9 ± 0.6 ka BP. The reason for this hiatus is not fully understood, but the preferred hypothesis is that at 133.1 ± 0.7 ka BP the glacier above Schafsloch had again become cold-based (Häuselmann et al., 2015), probably due to a short stadial prior to the onset of the Eemian. Calcite formed after 131.9 ± 0.6 ka BP is characterized by increasingly lower $\delta^{13}C$ values and rising $\delta^{18}O$ values, indicating incipient vegetation under a warming climate.

The early warming during Termination II captured by the Schafsloch stalagmite has been recorded by other speleothems. Several samples from Spannagel Cave show evidence of an early growth phase at 136.7 ± 2.8 ka (Spötl et al., 2002, 2007; Holzkämper et al., 2005). A stalagmite from Schneckenloch (entrance at 1285 m a.s.l.), located about 55 km

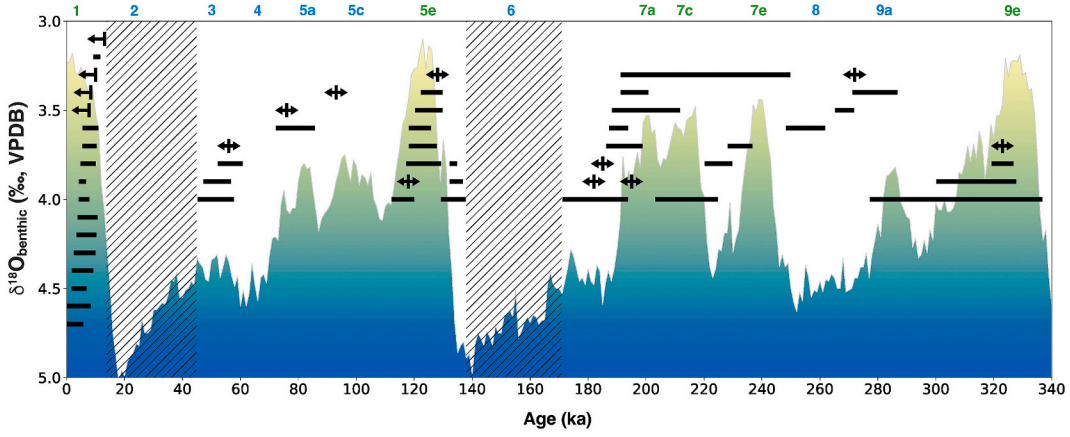

Fig. 7. Growth intervals of speleothems in Spannagel Cave and Kleegruben Cave. Each thin horizonal bar represents one speleothem (or one growth phase within a speleothem). Single arrows mark basal ages of in-situ stalagmites obtained by reconnaissance drilling. Double arrows show a single age in a small speleothem. The blue-green shaded background shows the deep-sea oxygen isotope stack LR04 (Lisiecki and Raymo, 2005). Prominent interglacial and glacial Marine Isotope Stages (MIS) are labelled in green and blue, respectively, on the top the panel (following Railsback et al., 2015). The hatched pattern marks intervals of no recorded speleothem deposition during MIS 6, late 3 and 2. Speleothem data sources: Spötl et al. (2002, 2007, 2008), Spötl and Mangini (2002, 2007, 2010), Fohlmeister et al. (2013), Holzkämper et al. (2004, 2005), Wendt et al. (2021), Spötl et al. (unpublished).

Fig. 8. Stalagmite 7H3 (40 cm in height) in 7H cave (left) and cut open and polished (right). It started to form at 22.9 ka BP and stopped at 14.7 ka BP. Photo left: M. Luetscher.

east of Schafsloch in western Austria (Fig. 5a), commenced growing at 134.1 ± 0.7 ka BP (Moseley et al., 2015) with high $\delta^{13}C$ values matching the local limestone, followed by a strong drop to slightly negative values at the onset of the Eemian. A very similar pattern was more recently reported from a stalagmite in Neotektonik Cave in Central Switzerland (entrance at 1727 m a.s.l.; Fig. 5a). This specimen started to grow at about 132 ka with high $\delta^{13}C$ (low $\delta^{18}O$) values, which decreased (increased) at the beginning of the Eemian (Wilcox et al., 2020). Schneckenloch and Neotektonik Cave developed in similar gray limestone and intercalated marl lithologies as Schafsloch, all of which contain disseminated pyrite. Collectively, these speleothem records suggest that at these sites the local MIS 6 glaciers were temperate at least by about 137 ka, allowing liquid water to exist in the karst fissure network beneath. This interstadial warming was synchronous within uncertainty with the initial rise in sea-surface temperatures in the North Atlantic at 136 ± 2.5 ka (Drysdale et al., 2009), which constitutes the principal moisture source of precipitation in the Alps.

The most recent work on subglacially formed speleothems centered again on caves in the Western Alps of Switzerland, in the area of Melchsee-Frutt. This karst region is located both below and above the tree line with multiple caves comprising tens of kilometers of passages. Research has focused mainly on Schratten Cave, Betten Cave and Neotektonik Cave (Fig. 5a and 10). In addition to stalagmites growing during MIS 1 (Leutz, 2014; Arps, 2017), MIS 5 (Wilcox et al., 2020), and MIS 7 and 9 (Skiba et al., 2023a), many stalagmites were identified by reconnaissance drilling and dating to have grown during glacial periods, including MIS 2, 3, 4, 6, 8, 10 and 12 (Fohlmeister et al., 2019; Fig. 11). Recently, a detailed study based on four stalagmites from Schratten and Betten Cave was published which represents one of the first precisely data proxy records in Europe covering the penultimate glacial period (MIS 6; Fohlmeister et al., 2023). Three specimens from Betten Cave grew at 1750 m a.s.l. and a fourth stalagmite from Schratten Cave was found at 1760 m a.s.l. Although the focus of this article was on the millennial-scale climate variability captured by these speleothems, their C isotopic composition (+3 to +6‰) argues for the absence of soil and vegetation in the catchment. Karst dissolution by sulfuric acid derived from the decomposition of pyrite is indicated by elevated sulfate concentrations in modern drip waters (unpublished). Given today's low temperatures in these caves (2.5–3.5 °C in Schratten Cave from 1990 to 2020), it is highly unlikely that speleothems would grow there continuously during full glacials such as MIS 6 without the thermal blanket of a warm-based glacier.

In a very recent paper, Skiba et al. (2023a) examined three stalagmites from Schratten and Betten Cave that show overlapping growth histories spanning 300 to 210 ka BP. Their $\delta^{13}C$ data suggest that the catchment of these two caves became glaciated at the transition from MIS 9 to 8 and remained continuously ice-covered throughout MIS 8. During MIS 7.5, 7.3, and 7.2, low $\delta^{13}C$ values suggest ice-free conditions and incipient Alpine vegetation, while during MIS 7.4, the glacier re-advanced and buried the cave sites (Skiba et al., 2023a). It is elucidating to compare these orbital-scale paleoglacier dynamics with data obtained from a stalagmite from Spannagel Cave. The latter specimen grew across MIS 7.5 to 7.1 without a hiatus, and its high and mostly positive $\delta^{13}C$ values suggest no significant soil development even during the MIS 7 warm phases (Wendt et al., 2021), consistent with the significantly higher elevation of this cave relative to those on Melchsee-Frutt.

No speleothem growth has been documented in Melchsee-Frutt caves during the LGM and second part of MIS 6e (Fig. 11). During the latter, speleothem growth ceased at 182 ka, about 2 ka after soil signals diminished, and resumed at 174.9 ka. The hiatus was interpreted to indicate cold-based glacier coverage coinciding with exceptionally low

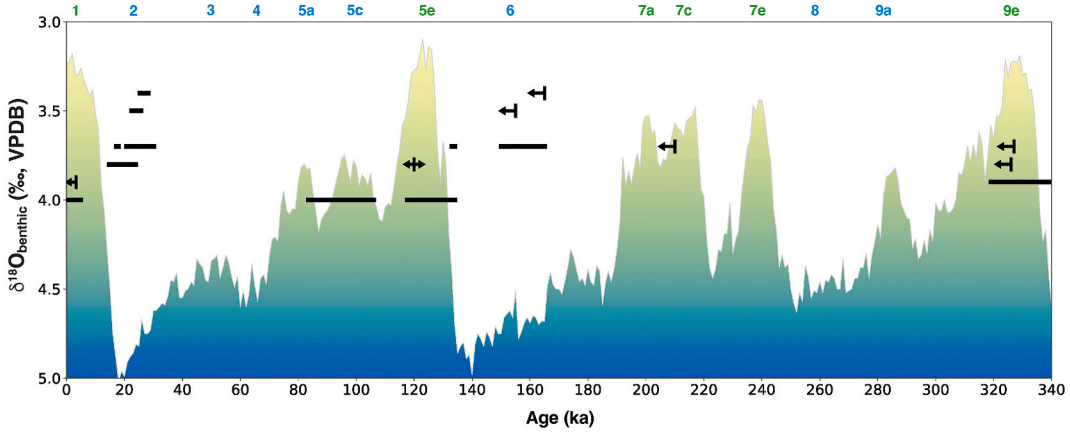

Fig. 9. Growth intervals of speleothems at 7H Cave. Each thin horizonal bar represents one speleothem (or one growth phase within a speleothem). Single arrows mark basal ages of in-situ stalagmites obtained by reconnaissance drilling. Double arrows show a single age in a small speleothem. The blue-green shaded background shows the deep-sea oxygen isotope stack LR04 (Lisiecki and Raymo, 2005). Prominent interglacial and glacial Marine Isotope Stages (MIS) are labelled in green and blue, respectively, on the top the panel. Speleothem data sources: Luetscher et al. (2015, 2021), Honiat (2018) and Luetscher (unpublished).

Fig. 10. Heavily corroded stalagmite continuing into a flowstone in the interior of Schratten Cave. According to reconnaissance drilling the base of this stalagmite is MIS 10 in age. Photo: C. Spötl.

summer insolation in the context of MIS 6 (Berger and Loutre, 1991). This conclusion is corroborated by other data suggesting a strong ice advance around this time (Dehnert et al., 2010) and a coeval speleothem growth hiatus in Spannagel cave (at 182.4 ka; Wendt et al., 2021).

Finally, Skiba et al. (2023b) inferred the presence of vegetated catchments (or the absence of glaciers) and the temperature at the base of such paleoglaciers from the growth history and C isotope composition of speleothems from twelve caves along the northern part of the Eastern and Western Alps, ranging in elevation from 870 to 2512 m a.s.l., and compared these data to modelled reconstructions of Alpine glaciers (Seguinot et al., 2018; Jouvet et al., 2023). Using a $\delta^{13}C$ threshold of −1‰ to indicate speleothems formed without pedogenic C input, this study found a good agreement between speleothem-derived soil presence/absence and modelled glacier coverage for the last glacial cycle.

6. Subglacial speleothems: A view beyond the European Alps

To date, no studies outside the European Alps (and the Columbia Icefield) have reported evidence of speleothem growth beneath glacier cover, but this result is unsurprising, given that few caves with dated speleothem records are located within or proximal to the LGM ice margins (Ehlers et al., 2011), let alone those of previous glacial advances. Here, we investigate candidate sites for subglacial speleothem records by overlaying the global karst map (Chen et al., 2017) with the LGM ice extent (Fig. 5).

One recent example comes from El Capitan Cave, located on Prince of Wales Island in Southeastern Alaska (Wilcox et al., 2019), which was previously ice covered and records discontinuous growth since MIS 5a. Speleothem growth intervals coincide with warm (and ice-free; Lesnek et al., 2020) phases of the Holocene and MIS 3, with notable hiatuses during MIS 2 and 4 that were attributed to permafrost development associated with ~5 °C reductions in regional temperature (based on the modern cave-air temperature; Wilcox et al., 2019). $\delta^{13}C$ values from −8 to −2‰ are indicative of contributions from soil-respired CO_2 and thus preclude a subglacial environment. Although the site falls within the western margin of the Cordilleran Ice Sheet (Fig. 5c), it is unlikely that future collections would yield evidence of subglacial growth, due to the absence of sulfide minerals in the host rock that could drive SAD.

In the Sierra Nevada range (California, USA), several caves proximal to the LGM extent of Pleistocene glaciation (Fig. 5c) have yielded speleothems ranging from MIS 6 to present, including Moaning Cave (520 m), McClean's Cave (300 m), and Crystal Cave (1386 m). Stalagmites from Moaning Cave (Oster et al., 2009, 2010) and McClean's Cave (Oster et al., 2014) exhibit growth from 16.5 to 8.8 ka and 67–55 ka, respectively, with a hiatus in the latter spanning the coldest phase of the last glacial (~55–17 ka). A multiproxy analysis of carbon-isotope systematics in Moaning Cave ruled out the presence of SAD and attributed high variability in dead-carbon fraction instead to the oxidation of aged soil-organic matter (Oster et al., 2010). Shelfstone deposits in Crystal Cave (and neighboring Weis Raum and Soldier's caves) indicate activity during MIS 5d (116.3 ka), the LGM (21.3 ka), and the Bølling-Allerød (14.7 ka) (Granger and Stock, 2004), while a survey of Sierra Nevada reported multiple ^{230}Th ages from MIS 6 and 2 (Stock et al., 2005). However, these sites are well below the paleo-ice margin (~3500 m a.s.l.; Granger and Stock, 2004), and no speleothem ages have yet been reported from higher elevation cave sites that were likely covered by an ice cap during the LGM (Stock et al., 2005).

Cave sites from the Midwestern USA are not candidates for recording subglacial speleothem growth, as they are generally found within an ice-free corridor between the southernmost lobes of the Laurentide Ice Sheet (Fig. 5c; Batchelor et al., 2019a). Instead, these sites have been utilized to map permafrost distribution in the periglacial zone. Although early investigations of Cold Water Cave, Iowa (Harmon et al., 1979) suggested

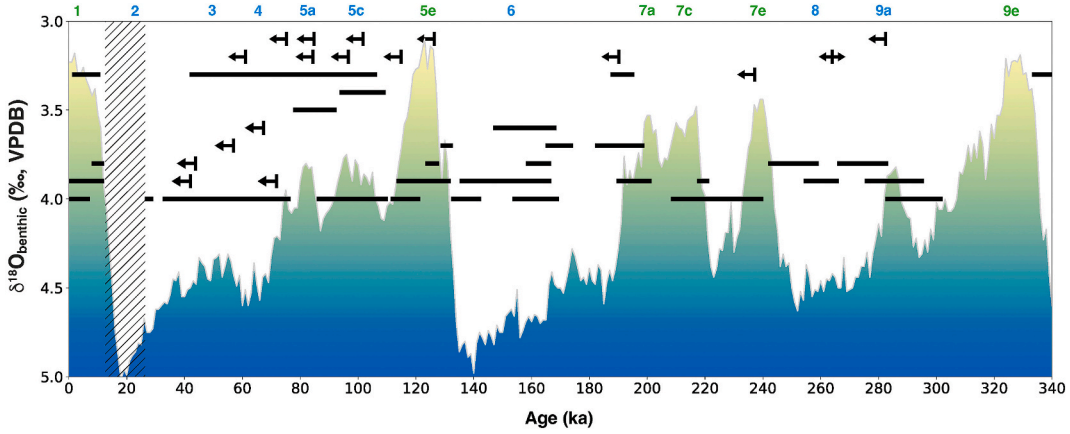

Fig. 11. Growth intervals of speleothems at Melchsee-Frutt (Betten Cave, Schratten Cave, and Neotektonik Cave). Each thin horizonal bar represents one speleothem (or one growth phase within a speleothem). Single arrows mark basal ages of in-situ stalagmites obtained by reconnaissance drilling. Double arrows show a single age in a small speleothem. The blue-green shaded background shows the deep-sea oxygen isotope stack LR04 (Lisiecki and Raymo, 2005). Prominent interglacial and glacial Marine Isotope Stages (MIS) are labelled in green and blue, respectively, on the top the panel. The hatched patterns mark two intervals of no recorded speleothem deposition during MIS 6 and 2. Speleothem data sources: Leutz (2014), Arps (2017), Fohlmeister et al. (2019, 2023), Wilcox et al. (2020), Skiba et al. (2023a, b).

continuous speleothem growth through the LGM, attempts to replicate these early alpha-spectrometrically measured ^{230}Th ages showed that growth began no earlier than ~11.4 ka (Alexander et al., 2001), consistent with the expected late glacial age of permafrost thaw. Based on the spatiotemporal distribution of ^{230}Th-ages from midwestern caves, intervals of perennial frozen ground were inferred from regional hiatuses in cave activity (esp. at 33–15 ka; Batchelor et al., 2019a), suggesting shorter and less extensive permafrost coverage during much of MIS 6 relative to MIS 2. Hence it is unlikely that any site experienced ice cover during previous glacial stages, with the exception of the MIS 6 maximum (Batchelor et al., 2019b).

A similar approach was applied to five caves along a meridional transect from Mongolia to central Siberia (Vaks et al., 2013, 2020), which fall well outside the LGM glacial extent in Asia but within or adjacent to modern permafrost boundaries (Fig. 5d). Here, speleothem growth is absent during all but interglacial stages, including the warm interstadials of the last glacial period (Vaks et al., 2013). The inception of Holocene growth in Botovskaya and Okhotnichya caves (~105°E) suggests permafrost degradation by ~9.9 ka, compared to 11.4 ka in Kyok-Tash Cave (86°E; Li et al., 2021) and 11.7 ka in Kinderlinskaya Cave (57°E; Baker et al., 2017), consistent with an eastward trend in postglacial warming and permafrost degradation that occurred almost ten millennia after initial retreat of the Eurasian ice sheets (Li et al., 2021). Among published datasets from northern Eurasia, only Kyok-Tash Cave is somewhat proximal to the LGM extent of mountainous glaciation (Fig. 5d) but is too low (890 m) to have been subjected to glacial cover, including at the MIS 6 maximum (Batchelor et al., 2019b). Still, the Altai and northern Ural regions are underexplored, and future collections from higher elevation (and higher latitude) caves may allow for a test of subglacial speleothem growth in central Russia.

Two high-elevation cave sites in western Asia exhibit geochemical proxy behavior consistent with subglacial conditions, despite falling outside of the mapped LGM limits of local ice extent: 1) Tonnel'naya Cave (3226 m), located in the westernmost ridges of the Tianshan Mountain Range (Cheng et al., 2016), and 2) Sarma Cave (2150 m), located in the Arabika plateau of the Western Caucasus range (Wolf et al., 2024). This apparent discrepancy presents a preliminary test for diagnostic criteria of subglacial speleothem growth (Sec. 7), as well as an opportunity to investigate whether an 'intermediate' phase can exist for sites without ice cover.

The observed temperature in Tonnel'naya Cave of 3.1 °C (Cheng et al., 2016) is low enough that LGM cooling likely resulted in subzero ground temperatures (3.8 °C cooling in MRI-CGCM3 at 3000 m elevation; Yukimoto et al., 2012). Common hiatuses in coeval stalagmites from ~14 to 36 ka (MIS 2), ~60–74 ka (MIS 4), and during MIS 3 and 5 stadials, are consistent with permafrost-induced cessation of infiltration during the coldest phases of the last glacial period. Growth was otherwise continuous through intervals from MIS 5d to MIS 3 that were plausibly characterized by mean annual air temperatures low enough to sustain local ice cover. Speleothem δ^{13}C ranges from approximately +1 to +7‰ and is generally higher than the host rock (2.6‰) during the last glacial period, which the authors attribute to a lack of vegetation on the high cuesta ridge and possible enrichment from PCP. However, it is difficult to explain continued speleothem growth in the absence of soil-respired CO_2 without an additional CO_2 source or dissolution pathway to sustain carbonate saturation. These proxy data are plausibly explained by ice or firn cover on the northwest-facing slope above the cave site, which could not only buffer ground temperatures from cold winter air (relative to the ice-free interglacials) but provide a steady influx of meltwater to facilitate sulfide-oxidation in the sediment interface and host rock. Additional proxies are needed, however, to distinguish between 1) the scenario proposed by Cheng et al. (2016), which explains elevated δ^{13}C and S/Ca through enhanced PCP and $CaSO_4$-rich dust during dry intervals; 2) permanent ice/firn cover above the cave that drove SAD in the absence of soil, resulting in subglacial speleothem deposition; and 3) possible intermediate conditions, by which variable contributions from SAD were induced by seasonal melt of the snowpack and may have complemented CAD from a thin soil cover (analogous to Corchia Cave, Italy; Bajo et al., 2017).

A recent study of low- and high-elevation cave sites in the Western Caucasus range contrasted speleothem proxy data from the Holocene with those from the LGM. Wolf et al. (2024) interpreted disproportionate LGM cooling/drying from the high-elevation record of Sarma Cave, which is currently 3–4 °C near the entrance and located below a sparsely vegetated Alpine catchment with thin soil cover. Model-reconstructed mean annual temperature was at least 3.6 °C colder during the LGM and thus may have resulted in discontinuous permafrost or ice cover above the cave. One major disparity between the Sarma Cave record and coastal sites around the Black Sea is the elevated δ^{13}C values during the LGM (0–3‰), which match or exceed local host rock values, potentially indicative of SAD. Both Sr/Ca and S/Ca ratios are highly elevated relative to Holocene values, consistent with enhanced PCP from SAD (Sec. 7.2) and analogous to the Tonnel'naya Cave record. To test whether high δ^{13}C and S/Ca values resulted from SAD or PCP-enrichment of a soil-carbon signal, two radiocarbon ages were obtained from stalagmite SAR-12-1 and yielded a Dead-Carbon Fraction (DCF) of 60% (Holocene) and 95% (LGM). While the Holocene DCF suggests a minor contribution from SAD (50% DCF is the theoretical maximum for a fully 'closed' system with CAD driven by contemporary soil CO_2; Hendy, 1971), the latter value is the highest reported for any speleothem and suggests that speleothem carbon derived almost entirely from the host rock. This combination of high δ^{13}C and DCF is only possible in a karst setting devoid of CAD (Sec. 7.5), leading the authors of that study to attribute LGM speleothem growth to sulfide oxidation and associated SAD.

Given the modelled LGM temperature of the cave site and inferred dissolution pathway, Sarma Cave plausibly represents an example of subglacial speleothem growth from the Western Caucasus. However, as with the previous example, Sarma Cave is located ~20 km southwest of the nearest mapped LGM glaciers (Fig. 5b). Although the catchment above the cave is at higher elevation than the lowest ice caps of this region, its relative proximity to the coastline results in much lower winter precipitation amounts (Bondyrev et al., 2015; Wolf et al., 2024). It therefore remains uncertain whether LGM ice cover existed but left no mappable features, or Sarma Cave represents a type of 'intermediate' phase in an ice-proximal setting. In light of these uncertainties, we propose a set of diagnostic criteria by which to distinguish subglacial environments in speleothem proxy data.

7. Multiproxy diagnostic criteria to identify subglacial speleothem growth

7.1. Stable-isotope signatures in subglacial settings

In caves where speleothem growth is driven by CAD, the carbon in speleothem calcite is derived principally from soil CO_2 and the dissolution of carbonate host rock (Hendy, 1971), with much lesser amounts from atmospheric CO_2 and the oxidation of sedimentary organic matter. The relative contribution of soil CO_2 ranges from 50% under closed carbonate dissolution conditions to nearly 100% in an open carbonate dissolution scenario. The temporal evolution of this value is related to precipitation (e.g., Fohlmeister et al., 2010; Griffiths et al., 2012; Noronha et al., 2014; Lechleitner et al., 2016) and other climatic parameters that modulate the amount of soil CO_2 via vegetative and soil microbial processes (Hendy, 1971; Fohlmeister et al., 2011, 2020), as well as the hydrology of the epikarst governing flow paths and gas exchange. Speleothem δ^{13}C is modified by mass-dependent fractionation during phase changes from the dripwater DIC reservoir, whose δ^{13}C falls along a mixing line between end member sources. Higher δ^{13}C values in speleothems are thus interpreted, generally, to result from reductions in temperature, precipitation, or vegetative cover that enhance the contribution of host-rock carbon to the drip DIC or the degree of

Rayleigh ^{13}C enrichment from PCP (McDermott, 2004; Fairchild et al., 2006).

When sulfide minerals (e.g., pyrite, FeS_2) are present in the sediment or host rock, oxidation may occur under a range of redox states, depending on the availability of $O_{2(aq)}$, Fe^{3+}, or NO_3 as the dominant oxidants (Bottrell and Tranter, 2002; Wynn et al., 2006; expanded discussion in Sec. 7.4). Because the sulfuric acid produced by this reaction is neutralized by dissolution of carbonate host rock, the resulting DIC reservoir is characterized by fractions resulting from the two dissolution pathways (CAD vs. SAD; Bajo et al., 2017), where enhanced SAD increases the relative contribution of DIC from the host rock, in place of soil CO_2, and thus speleothem $\delta^{13}C$. For example, Bajo et al. (2017) utilized proxy system modeling to find that a Holocene stalagmite from Corchia Cave, Italy, grew under variable contributions from SAD (up to 40%, relative to CAD), which was reflected in high $\delta^{13}C$ values (up to ~2.5‰) that exceeded the host rock composition. The amount of initial Ca^{2+} lost to PCP (~60%) was constrained by Mg/Ca and estimated to have increased speleothem $\delta^{13}C$ by 3–4‰.

For subglacial settings, we can hypothesize that the CAD contribution to the DIC is negligible, compared to the Corchia Cave example, and should invariably lead to speleothem $\delta^{13}C$ values within range of (or higher than) the host rock $\delta^{13}C$. In the absence of soil, however, dissolved atmospheric CO_2 and oxidation of pre-aged organic matter can still lead to small but quantifiable reductions in $\delta^{13}C$ from CAD (e.g., Tranter et al., 1997; Oster et al., 2010). Increased $\delta^{13}C$ from kinetic effects or PCP can also partially offset the soil-CO_2 signature in settings with thin soil cover or reduced biological activity (Cheng et al., 2016; Skiba et al., 2023b), which could be mistaken for SAD. These caveats warrant caution when applying $\delta^{13}C$ as a proxy for glacier cover, because although it may be a prerequisite for identification of subglacial speleothem growth, high $\delta^{13}C$ values are not uniquely diagnostic. One solution is to apply a 'correction' to the speleothem $\delta^{13}C$ signal by utilizing major cation data to constrain the amount of PCP and calculate the initial $\delta^{13}C$ of the DIC pool (Skiba and Fohlmeister, 2023). Comparing these values against that of the host rock, one can then determine whether growth may have proceeded within a predominantly SAD system.

In addition to high $\delta^{13}C$, subglacial speleothem records should also exhibit relatively low $\delta^{18}O$, due to recharge from glacial meltwater in high-latitude or Alpine settings. These settings are characterized by the accumulation of predominantly cold-season precipitation that is subject to Rayleigh distillation processes along cold air trajectories and/or high elevation changes, which collectively leads to low $\delta^{18}O$ values (Bowen and Wilkinson, 2002; Bühler et al., 2021). Glacier cover is also biased toward intervals of colder global climate, associated with lower $\delta^{18}O$ in precipitation, especially at mid to high latitudes.

7.2. Stable isotope fractionation effects in high-Alpine cave systems

Low-temperature caves have been considered to be less prone to kinetic effects on $\delta^{18}O$ during carbonate precipitation (Spötl and Mangini, 2002; Mangini et al., 2005; Spötl et al., 2006; Vollweiler et al., 2006). In cold, high-elevation settings, carbonate dissolution is usually weaker compared to warmer low-elevation settings due to lower soil CO_2 concentrations. This leads to a lower CO_2 supersaturation of the water dripping in the cave, resulting in a lower potential for calcite or aragonite supersaturation and smaller precipitation rates. Early modelling studies have shown that low temperatures limit fractionation-induced disequilibrium effects for stable oxygen and carbon isotopes when the drip rate is high (e.g., Mühlinghaus et al., 2009; Scholz et al., 2009; Deininger et al., 2012) due to slower degassing and precipitation reactions (Dreybrodt and Scholz, 2011). Additionally, low carbonate precipitation rates lead to only small variations in the degree of kinetic effects during the $\delta^{18}O$ fractionation process when precipitation rate is changing (e.g., Coplen, 2007; Dietzel et al., 2009; Hansen et al., 2019). Recently, more sophisticated proxy system models support this interpretation of smaller disequilibrium effects when temperatures are lower when accounting for PCP, which prolongs the water-cave atmosphere contact time before the drop is reaching the top of the speleothem (Guo and Zhou, 2019). When PCP occurs, disequilibrium effects begin to modulate the final $\delta^{18}O$ and $\delta^{13}C$ composition of precipitated carbonate, albeit to a lesser extent at lower temperature relative to warmer cave environments (Guo and Zhou, 2019).

In addition, speleothem records from Alpine caves with low present-day temperatures provide another important advantage for their use in environmental studies. Present-day temperatures in Alpine caves are typically less than a few degrees Celsius. As liquid water must have been present even during glacial periods recorded by the speleothem growth, karst and cave temperatures were not lower than 0 °C and thus similar to today. Hence, changes in temperature-related isotope fractionation were minimal even during strong atmospheric temperature differences associated with interstadial-stadial and interglacial-glacial transitions. This constraint would allow for a more straightforward evaluation of $\delta^{18}O$ in the drip water and meteoric precipitation e.g., by inverse modeling (Wackerbarth et al., 2010; Fohlmeister et al., 2017, 2023; Skiba et al., 2023a; Wolf et al., 2024) than in warmer non-Alpine caves.

The oxidation of sedimentary sulfides in the host rock, however, can strongly enhance disequilibrium fractionation during subglacial speleothem growth. Generally, SAD of the carbonate host rock leads to higher initial Ca^{2+} concentrations in the drip water than under CO_2-driven carbonate dissolution (Dreybrodt, 1988; Owen, 2017), resulting in a higher oversaturation of the water with respect to cave-air CO_2 and an increased amount of PCP, assuming no offsets from hydrological shifts (Spötl and Mangini, 2007; Spötl et al., 2006; Skiba et al., 2023a). In addition, the rate of isotopic exchange processes (with water and cave air CO_2) is slower in low temperature environments (Dreybrodt and Scholz, 2011; Guo and Zhou, 2019; Deininger et al., 2021; Skiba and Fohlmeister, 2023). Therefore, re-equilibration of the stable isotope composition of the water after PCP is slow and fractionation-induced isotope enrichment will ultimately be recorded by speleothems originating from sulfuric-acid dissolution.

Such disequilibrium effects can still be helpful for event detection, i.e. stadial-interstadial transitions, if PCP varies with climate in a way that enhances the initial climate signal and thus the signal-to-noise ratio. Also, these disequilibrium effects are linked to local (i.e., glacier-related) processes, as PCP changes on stadial-interstadial timescales are related to glacier meltwater variability (Skiba et al., 2023a). Although enhanced PCP during cold (low $\delta^{18}O$) phases could mute millennial-scale $\delta^{18}O$ variability—highlighting the importance of constraining PCP through proxy system modelling—climate signals on multi-decadal and longer timescales are well documented in speleothems from Alpine cave sites (e.g., Spötl et al., 2006; Luetscher et al., 2015; Fohlmeister et al., 2023; Skiba et al., 2023a).

7.3. Cluster analysis of paired $\delta^{13}C/\delta^{18}O$ data in speleothem records

To evaluate the pairing of $\delta^{13}C/\delta^{18}O$ as a proxy for subglacial speleothem growth, we conducted a density and cluster analysis of speleothem records in the SISALv2 database (Speleothem Isotopes Synthesis and Analysis; Comas-Bru et al., 2020), which we have supplemented here by recently published data from Alpine speleothems (Fohlmeister et al., 2023; Skiba et al., 2023a; Wolf et al., 2024). A total of 300,444 paired stable-isotope data from 309 cave sites comprise this analysis, the majority of which plot in a narrow range from −3 to −7‰ ($\delta^{18}O$) and −7 to −10‰ ($\delta^{13}C$) (Fig. 12a and b). Applying a Gaussian mixture model assigns the probability that each data point belongs to one of eight centroids or 'clusters' (Fig. 12c), fitted heuristically to the data through a k-means++ algorithm in Matlab and depicted by 2-σ ellipses. This approach consistently results in a centroid (Cluster 5) that is defined by high $\delta^{13}C$ (+3.9‰) and low $\delta^{18}O$ (−11.0‰), as long as 8 or more components are designated to run the model. With fewer components, clusters 5 and 6 tend to combine and encompass such a wide

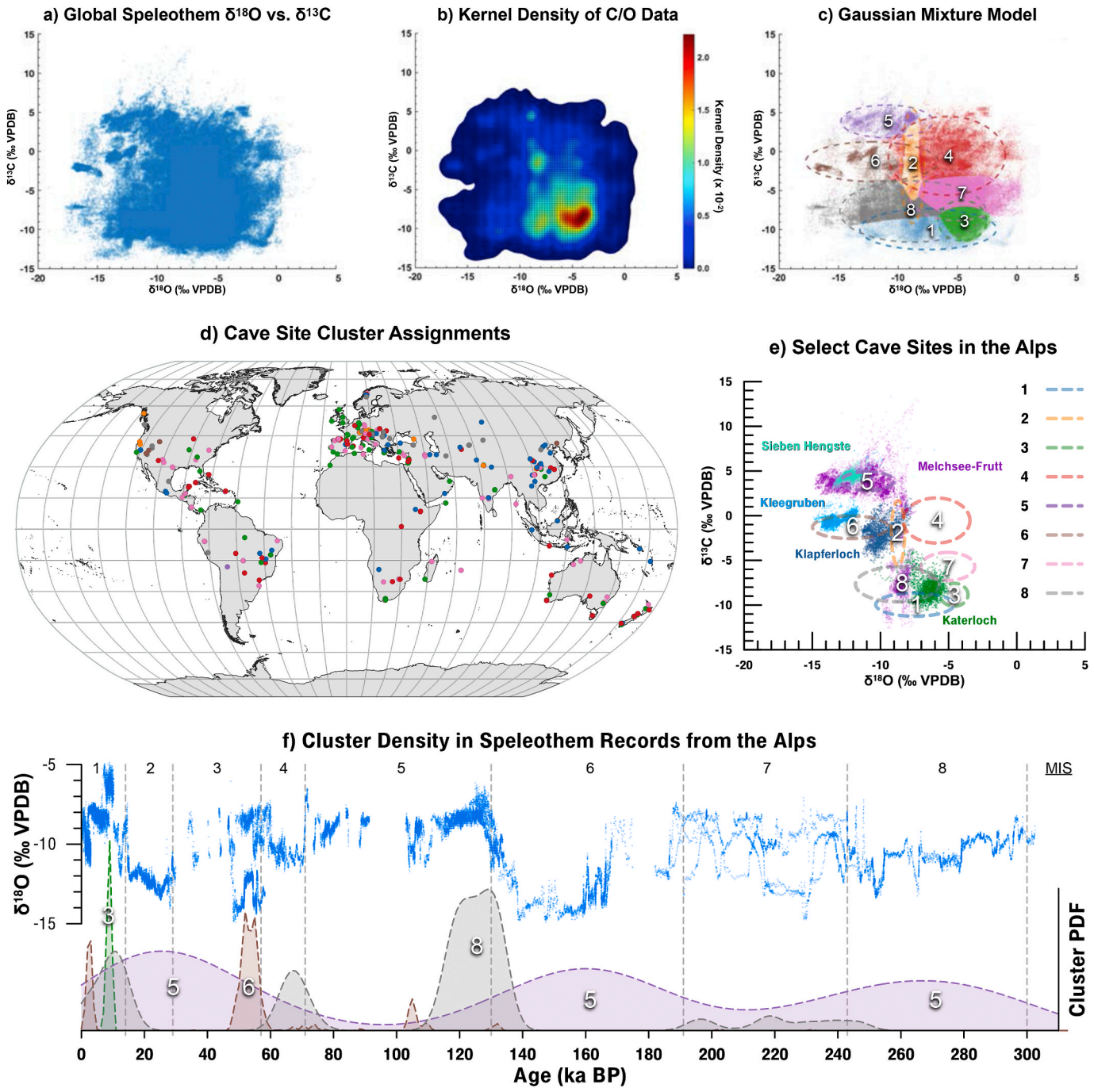

Fig. 12. Application of cluster analysis of global speleothem $\delta^{13}C/\delta^{18}O$ to the European Alps. (a) Cross plot of all paired $\delta^{13}C/\delta^{18}O$ data in the SISALv2 database, in addition to recently published data from Melchsee Frutt (Skiba et al., 2023a; Fohlmeister et al., 2023) and Sarma Cave (Wolf et al., 2024). (b) Kernel density plot of the data in (a); (c) Cluster analysis using a Gaussian mixture model and 8 components. Centroids are numbered arbitrarily by the algorithm. Dashed ellipses show the 2-σ range of each mixture model. (d) Global map of cave sites included in the analysis, color-coded according to the highest number of cluster assignments. (e) Cross plot of data from representative sites in the Alps region: Sieben Hengste, Melchsee-Frutt, and Kleegruben (high elevation, ice-covered during major glacial advances); and Klapferloch and Katerloch (low elevation, ice-free). Dashed ellipses show the 1-σ range of mixture models. (f) Composite of $\delta^{18}O$ data from all published speleothem records from the Alps region (blue). Shaded curves show the temporal frequency of cluster assignments in the Alps subset using a kernel probability density function (PDF). The vertical axis of each PDF has been scaled arbitrarily for visual clarity.

range of values that the model lacks explanatory power. If more than 8 components are designated, the results are similar to Fig. 12c, except that additional clusters are defined from data in the lower right quadrant.

Next, we tested whether clusters in the $\delta^{13}C/\delta^{18}O$ space are coherent with cave geography (spatial) and ambient climate (temporal), such that a robust 'subglacial cluster' may be defined. Each of the 309 caves was assigned to one of eight clusters, based on which cluster captured the highest number of individual $\delta^{13}C/\delta^{18}O$ measurements from that site (Fig. 12d). While this approach introduces several biases, for example in caves where growth is limited to warmer/wetter intervals, a few key patterns emerge. Nearly half of caves fall into cluster 3 (23%) and 7 (24%), which have median site elevations of 220 m and 350 m, respectively. Relatively few caves fall into clusters 2 (4%), 5 (2%), and 6

(2%), but these are characterized by much higher median site elevations of 1285 m, 1890 m, and 2165 m. Of these high-elevation groups, only Cluster 5 exhibits $\delta^{13}C$ values above that typical for marine carbonate bedrock, thus consistent with a predominantly SAD system and most likely to be diagnostic of subglacial speleothem growth.

Five cave sites were assigned to Cluster 5, of which three (Schratten, Schafsloch, and Sieben Hengste) are located in the Alps and have been interpreted as hosting subglacial speleothem records (Fig. 12a; Häuselmann et al., 2015; Luetscher et al., 2021; Skiba et al., 2023b). The other two (Chiflonkhakha, Sahiya) are located in the Andean and Himalayan ranges, respectively, but report only Late Holocene data inconsistent with glacier cover (Apaéstegui et al., 2018; Sinha et al., 2015). Thirteen cave sites contain 1–20% of paired $\delta^{13}C/\delta^{18}O$ values assigned to Cluster 5, including Hölloch, Spannagel, Schneckenloch, Neotektonik, Kleegruben, Gassel, Tonnel'naya, and Sarma (Fig. 12a and b), which have been interpreted as having subglacial growth intervals (discussions herein and Skiba et al., 2023b). The remaining caves (Huagapo, Minnetonka, Cesare Battisti, and Pacupahuain) are high-elevation sites (1880–3850 m a.s.l.) that lack glaciation but potentially could be driven by SAD from intense snowmelt through thin or patchy Alpine vegetation cover. To illustrate these geographic controls specifically for the European Alps, we have plotted data from three predominantly subglacial cave sites (Schratten/Betten/Neotektonik, grouped as Melchsee-Frutt, Sieben Hengste, and Kleegruben) and two non-glacial caves (Klapferloch and Katerloch) over the 1-σ cluster ellipses (Fig. 12e). These patterns are broadly consistent with our interpretation of the Gaussian mixture model but importantly show that during glacial retreats (e.g. MIS 3 interstadials and MIS 5e), the $\delta^{13}C/\delta^{18}O$ behavior of subglacial cave sites can shift toward (non-glacial) clusters 2, 6, and 8.

Finally, we test for a robust temporal signal associated with ambient regional climate in the Alps (Fig. 12f). A kernel probability density function was calculated for each cluster, based on individual assignments to the 45,617 paired $\delta^{13}C/\delta^{18}O$ data available for the Alps. Consistent with our hypothesis, the frequency of Cluster 5 assignments is higher during glacial periods (MIS 2, 6, and 8), while the frequency of data in clusters 3, 6, and 8 is generally higher during warm phases (MIS 1, 3, 5e, and 7). The high frequency of Cluster 6 during early MIS 3 derives from the fact that Kleegruben stalagmites span several stadial-interstadial cycles (Spötl et al., 2006) and thus oscillate between clusters 6 (non-glacial, high-altitude) and 5 (subglacial). We conclude that paired $\delta^{13}C/\delta^{18}O$ values provide a robust first-order proxy that captures speleothem growth in subglacial settings, with the caveat that non-glaciated cave sites in Alpine settings can exhibit the same signal. Thus additional criteria are required for a definitive environmental interpretation.

7.4. Identifying SAD from paired $\delta^{34}S/\delta^{18}O$ analysis of speleothem sulfate

Characterization of speleothem sulfur can elucidate biogeochemical cycling and redox conditions within the soil-karst-cave system, due to its mobility through the system, relative solubility at a range of pH/Eh, and ability to be incorporated into minerals as carbonate-associated sulfate (CAS) (Frisia et al., 2005; Wynn et al., 2008; Fairchild and Treble, 2009; Wynn et al., 2018). In most ecosystems, the primary source of soil-zone S is the atmospheric deposition of sulfate, which is subsequently reduced and predominantly stored as organic matter in C–S compounds, whereas weathering inputs tend to be minor (Borsato et al., 2015). Additionally, oxidation of organic matter and associated desorption of sulfate compounds contributes highly mobile sulfate anions to the soil-sulfate pool. Fast sulfate transport through the epikarst may connect the cave system to soil-zone dynamics at multiannual to decadal scales, depending on the extent of S cycling (Borsato et al., 2015). Sulfate concentrations in drip water and speleothem calcite are known to covary with the amount of PCP, resulting in enhanced S/Ca, and the abundance of defect sites during mineral growth, which is related to the calcite precipitation rate. The latter effect can result in a seasonal S/Ca signal that follows cave-air pCO_2, despite stable drip water concentrations (Borsato et al., 2015; Wynn et al., 2018).

Sulfate ions are generally stable in karst settings during transport and retain their soil-zone isotopic composition (Taylor and Wheeler, 1994), due to limited exchange with groundwater (Bottrell, 2007), making them effective tracers of S sources and surface processes. The isotopic composition of aqueous sulfate ($\delta^{34}S$) ultimately derives from an admixture of four principal end members (Mitchell et al., 1998; Wynn et al., 2008): 1) atmospheric sulfate, comprising marine (15–20‰), volcanic (0‰), and industrial (−3 to +9‰) aerosols; 2) terrestrial biogenic S (−30 to 0‰); 3) weathering of CAS and evaporites (10–40‰); and 4) oxidation of sedimentary sulfides (−50 to +15‰). The wide range in sedimentary $\delta^{34}S$ and much lower values of sulfides reflects the large (up to 40‰) and highly variable fractionation associated with sulfate reduction, particularly when biomediated in limiting environments, and concomitant $\delta^{34}S$ evolution of the marine sulfate reservoir through geologic time (Present et al., 2020). Importantly, the $\delta^{34}S$ of respective end members can and should be constrained for the given study area to construct source mixing models with higher precision (e.g., Bottrell, 2007; Wynn et al., 2013; Sun et al., 2017). This approach is routinely used to identify relative contributions to dissolved sulfate in aquifers and specifically to detect for sulfide (esp. pyrite) oxidation, given its influence on groundwater quality (e.g., Taylor and Wheeler, 1994; Samborska et al., 2013; Chen et al., 2023).

Glacial meltwater is potentially a source of oxidizing recharge to the ice-rock interface and underlying karst aquifer. Although subglacial environments tend to remain suboxic outside of summer recharge, certain dissolved ions and microbial activity can facilitate sulfide oxidation in the absence of O_2 (Tranter et al., 1997; Bottrell and Tranter, 2002; Wynn et al., 2006; Hodson et al., 2008), which provides sulfuric acid leading to bedrock dissolution and thus enabling speleothem growth without inputs from a CO_2-rich soil cover. Oxidation proceeds by the following pathways (Taylor and Wheeler, 1994):

$$FeS_2 + \frac{7}{2}\,O_2 + H_2O \rightarrow Fe^{2+} + 2SO_4^{2-} + 2H^+ \quad (1)$$

$$Fe^{2+} + \frac{1}{4}O_{2(aq)} + H^+ \rightarrow Fe^{3+} + \frac{1}{2}H_2O \quad (2)$$

$$FeS_2 + 14Fe^{3+} + 8H_2O \rightarrow 15Fe^{2+} + 2SO_4^{2-} + 16H^+ \quad (3)$$

Each mole of oxidized pyrite (FeS_2) contributes 2 moles of sulfuric acid (H_2SO_4) to the system, which subsequently drive carbonate dissolution and potentially add 4 mol of Ca^{2+} + Mg^{2+} and bicarbonate (HCO_3^-):

$$2Ca_xMg_{(1-x)}CO_3 + H_2SO_4 \rightarrow 2_xCa^{2+} + 2_{(1-x)}Mg^{2+} + 2HCO_3^- + SO_4^{2-} \quad (4)$$

If organic matter is present, such as from sediments, oxidation may be facilitated by the sulfate produced in reactions 1–4:

$$2CH_2O + SO_4^{2-} + H^+ \rightarrow HS^- + 2H_2O + 2CO_2 \quad (5)$$

Because fractionation ($\Delta^{34}S$) during sulfide oxidation and co-precipitation with calcite are both small (Taylor and Wheeler, 1994; Canfield, 2001; Barkan et al., 2020), a linear mixing model can be defined from the final $\delta^{34}S_{SO4}$ of drip water and speleothem calcite to approximate contributions from pyrite oxidation, assuming the composition of sedimentary sulfide ($\delta^{34}S_{FeS2}$) and soil-zone sulfate ($\delta^{34}S_{soil}$) can be reasonably constrained:

$$\delta^{34}S_{SO4(aq)} = x \cdot \delta^{34}S_{soil} + (1-x) \cdot \delta^{34}S_{FeS2} \quad (6)$$

Even a 10% novel contribution from pyrite oxidation would result in a negative $\delta^{34}S$ anomaly of 1.8‰–4‰, assuming a $\Delta^{34}S_{soil-FeS2}$ of 18‰ (Phanerozoic mean) or 40‰ (maximal), respectively. Much higher anomalies are observed in aquifers where pyrite oxidation may result in

a 2–10-fold increase in [$SO_{4(aq)}$] and contribute >50% of groundwater sulfate (e.g. Samborska et al., 2013). We emphasize, however, that the equation assumes only two end members and no influence from mass-dependent fractionation, which is an oversimplification of S cycling. Under persistent reducing conditions (e.g. with enhanced soil activity and/or the presence of sulfate-reducing bacteria), preferential reduction of $^{32}SO_4$ can increase $\delta^{34}S$, even to the point of exceeding bedrock values, in the residual $SO_{4(aq)}$ recorded by speleothem calcite (Wynn et al., 2013). Similarly, shifts in the relative contribution of atmospheric vs. biogenic sulfur to soil SO_4 (resulting from climatic or ecological change) can modify the signal without any change in the degree of sulfide oxidation (Mitchell et al., 1998). We propose that this oversimplification can be addressed by coupling speleothem $\delta^{34}S$ data with the following: 1) comparison to the speleothem $\delta^{34}S$ baseline for each climatic state; 2) analysis of speleothem S/Ca; 3) comparison to speleothem $\delta^{13}C$; 4) if applicable, analysis of the dead carbon fraction (DCF); and 5) analysis of speleothem $\delta^{18}O_{SO4}$.

Characterization of speleothem $\delta^{34}S_{SO4}$ under warm/cold phases (inferred from speleothem $\delta^{18}O$) provides a baseline against which to test for anomalies resulting from the above processes, because it should represent the equilibrium value of soil-zone $\delta^{34}S_{SO4(aq)}$ for a given climatic normal (affecting soil activity, weathering rates, and redox state in the karst zone). Negative $\delta^{34}S$ anomalies from pyrite oxidation can be differentiated from enhanced biogenic S contribution in that the former should occur coevally with positive S/Ca and $\delta^{13}C$ anomalies, reflecting a substantial increase in aqueous sulfate (eqs. (1)–(4)) and SAD of bedrock. Because SAD increases the fraction of groundwater alkalinity derived from bedrock dissolution, the DCF of speleothem calcite will concomitantly increase to >50% (Sec. 7.5).

Finally, redox conditions at the time of speleothem growth can be assessed from the analysis of $\delta^{18}O$ in speleothem CAS, since oxygen atoms in SO_4^{2-} are derived unequally from dissolved oxygen and H_2O (stoichiometric ratio of 7:1 in Eq. (1)) and each has a unique enrichment factor (ε) (Taylor and Wheeler, 1994). When free oxygen is limited (low f_{O2}), $\delta^{18}O_{SO4}$ approaches $\delta^{18}O_{H2O}$ as sulfate derives nearly all its oxygen from water or nitrates (Sun et al., 2017), whereas $\Delta\delta^{18}O_{(SO4-H2O)}$ typically exceeds ~8‰ under aerobic oxidation of sulfides, according to the mass-balance equation (Fig. 13):

$$\delta^{18}O_{SO4} = x\cdot\left(\delta^{18}O_{H2O} + \varepsilon_{H2O}\right) + (1-x)\left(\delta^{18}O_{O2} + \varepsilon_{O2}\right) \quad (7)$$

Here, the $\delta^{18}O$ of atmospheric oxygen ($\delta^{18}O_{O2}$ = 23.8‰) and enrichment factor for water (ε_{H2O} = 4‰) are well known. For speleothem-based applications, however, $\delta^{18}O_{H2O}$ must be approximated from $\delta^{18}O_{calc}$ (if temperature is known) and/or fluid-inclusion analysis. The enrichment factor for dissolved oxygen (ε_{O2}) is −4.3‰ in sterile reactions and up to −11.4‰ in the presence of *Acidithiobacillus ferrooxidans*, but typically close to −8.7‰ in neutral to alkaline natural environments (Taylor and Wheeler, 1994). If these parameters are constrained, we can theoretically use $\Delta\delta^{18}O_{(SO4-H2O)}$ to differentiate between subglacial and non-glaciated systems driven by SAD, because the latter is almost exclusively fed by well-mixed, oxygen-rich meteoric water. Conversely in subglacial systems, sulfide oxidation largely occurs within oxygen-depleted basal flow environments that characterize the ice-sediment interface (Hodson et al., 2008), which results in lower $\delta^{18}O_{SO4}$, especially during winter (Tranter et al., 1997; Wynn et al., 2006; Graly et al., 2018). Because basal reservoirs are seasonally recharged with oxic meltwater from the glacier surface via moulins (causing glacial discharge to exhibit a seasonal fO_2 and $\delta^{18}O_{SO4}$ signal; Wynn et al., 2006), the mean redox state of the sulfide-oxidation pathway also depends on hydraulic connectivity with the surface environment and the respective melting rates. Thus, we should expect $\Delta\delta^{18}O_{(SO4-H2O)}$ to increase progressively with thinning, disintegration, and eventual retreat of the glacier, as these processes alleviate the redox gradient between the supra- and subglacial environment (Hodson et al., 2008).

We propose this multiproxy analysis of speleothem sulfate as a diagnostic criterion for identifying speleothem growth under subglacial conditions. In the absence of CO_2-rich soils and microbial activity, extensive pyrite oxidation within the system should: 1) lower pH and/or buffering capacity from the production of sulfuric acid; 2) facilitate SAD of carbonate bedrock; 3) substantially increase the contribution of bedrock to the groundwater DIC reservoir, increasing $\delta^{13}C$ and DCF; 4) lower the $\delta^{34}S$ of groundwater SO_4 toward that of host-rock pyrite; 5) enhance groundwater sulfate concentration and hence speleothem S/Ca; and 6) release Fe and trace metals commonly bound in pyrite, such as Cu and As (Sun et al., 2017), which might also be detectable in speleothem calcite.

Despite its relevance to climatic and ecological processes in karst systems, sulfur is not routinely analyzed in speleothem paleoclimatology. Sulfur concentration is occasionally utilized as a proxy for PCP or atmospheric perturbations from volcanic or industrial emissions, and sulfur-isotope data are available only from a handful of studies, which primarily examined the recent anthropogenic signal (e.g., Frisia et al., 2005; Borsato et al., 2015). One drawback of sulfate-isotope analysis ($\delta^{34}S_{SO4}$ and $\delta^{18}O_{SO4}$) is that it destructively requires large amounts of calcite material (commonly 100–200 mg, depending on the S concentration), limiting the temporal resolution of stable-isotope data from CAS, especially in slow-growing stalagmites.

7.5. Dead-carbon fraction in subglacial speleothem calcite

Similar to $\delta^{13}C$ in speleothem calcite, radiocarbon activity ($a^{14}C$)

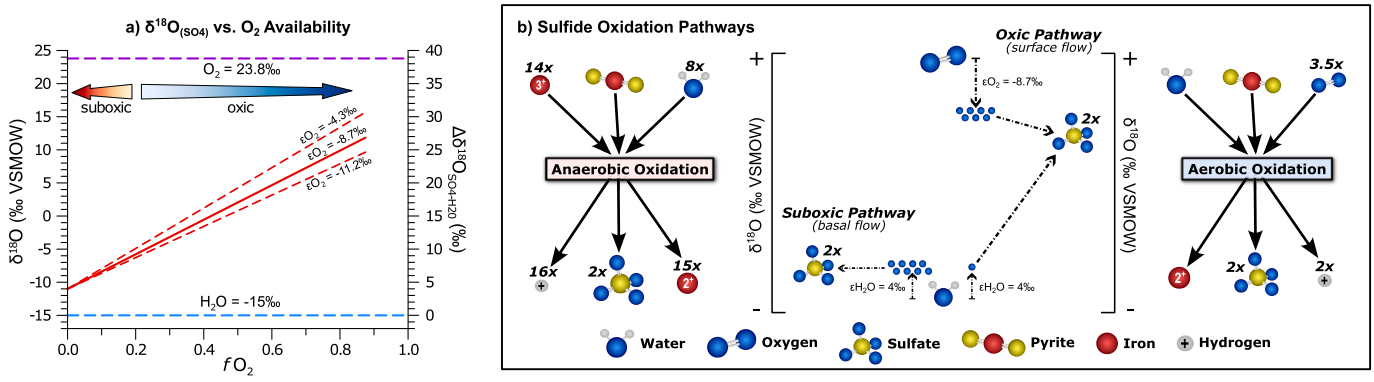

Fig. 13. Impact of oxygen availability on sulfate $\delta^{18}O$. (a) Mixing lines between aerobic and anaerobic pyrite oxidation, assuming $\delta^{18}O_{water}$ = −15‰ (typical of Alpine precipitation). Dashed lines denote range of possible enrichment factors (ε) between atmospheric and sulfate oxygen. (b) Schematic of reactive pathways for sulfide oxidation under oxic and anoxic conditions, which respectively may characterize surface and basal conditions. Center frame explains the resulting $\delta^{18}O$ of sulfate due to the respective enrichment factors and stoichiometric contributions from O_2 and H_2O.

depends on the $^{14}C/^{12}C$ ratio of carbon sources and modification by mass-dependent fractionation along pathways. In the standard cave model driven by CAD, the relative C contribution to dripwater HCO_3^- from soil CO_2 ranges between theoretical end members of nearly 100% (open system, where the water remains in contact with the soil-CO_2 reservoir during carbonate dissolution and maintains its isotopic composition) to 50% (closed system, where the water is not in contact with soil CO_2) (Hendy, 1971). The latter scenario results in higher $\delta^{13}C$ for dripwater HCO_3^- by ~2–3‰, depending on soil pCO_2 and the $\delta^{13}C$ of plant matter and host rock. However, $a^{14}C$ proportionally declines with increasingly closed conditions from being in equilibrium with the soil CO_2 reservoir ($a^{14}C_{HCO3} \cong a^{14}C_{atm}$) to 50% the activity of contemporary atmosphere in a perfectly closed system, due to the contribution of ^{14}C-free carbonate ions from bedrock. The $a^{14}C$ of DIC is further subject to the same processes that influence $\delta^{13}C$ via mass-dependent fractionation, such as diffusion of CO_2, PCP, and drip degassing (Hendy, 1971; Genty et al., 2001; Bajo et al., 2017). Based on the final ratio between $a^{14}C$ of speleothem calcite and atmosphere at the time of formation (t), the percentage of 'dead carbon' (dead-carbon fraction, DCF) can be calculated as follows (Genty et al., 2001; Bajo et al., 2017):

$$DCF(t) = \left(1 - \frac{a^{14}C_{calc}(t)}{a^{14}C_{atm}(t)}\right) \cdot 100\% \quad (8)$$

Where $a^{14}C_{calc}(t)$ is the initial value in speleothem calcite, estimated from the decay since the ^{230}Th-age (t) of the sample ($\lambda = 1/8267\ y^{-1}$):

$$a^{14}C_{calc}(t) = \frac{a^{14}C_{measured}}{e^{-\lambda t}} \quad (9)$$

And where $a^{14}C_{atm}$ is the atmospheric radiocarbon concentration determined for time (t) using the radiocarbon calibration curve (IntCal20; Reimer et al., 2020). Thus in cave systems controlled by CAD, the speleothem DCF theoretically ranges from ~0% to 50%.

Values of DCF can exceed 50% either when 1) some amount of CO_2 is sourced from the oxidation of pre-aged organic matter, whose $a^{14}C$ is less than contemporary atmosphere; or 2) bedrock dissolution is facilitated by some process other than CAD, such as SAD. Although both processes enhance speleothem DCF, their respective influences on $\delta^{13}C_{DIC}$ are opposite. Because the $\delta^{13}C$ of stored sedimentary and soil organic matter is typically near or less than that of soil CO_2, $\delta^{13}C_{DIC}$ should remain stable, if not decrease, in response to contributions from aged organic matter to the epikarst DIC reservoir. This process may occur irrespective of the bedrock-dissolution pathway.

Conversely, carbonate dissolution by sulfuric acid generates 2 mol of 'radiocarbon-dead' HCO_3^- (eq. (4)) with $\delta^{13}C$ values that typically range from −2 to +6‰ for Phanerozoic bedrock. Increasing degrees of SAD should therefore shift both $\delta^{13}C_{DIC}$ and DCF linearly toward the end-member composition of the local host rock. Combining this isotope mixing model with modern constraints from drip water chemistry, Bajo et al. (2017) estimated a ~20% contribution to DCF from SAD in Corchia Cave, Italy, where modern drip water had a DCF of approximately 60%. The remaining ~40% came from CAD, signifying a nearly closed system, which likely is related to relatively low soil pCO_2 associated with a thin soil zone in the Alpine catchment. More extreme values of DCF can be predicted for subglacial speleothems, which grow in the total absence of a soil zone and thus minimal contributions from CAD. Although these data are not available for any published records of speleothems identified as subglacial, the LGM growth interval of stalagmite SAR-12-1 from Sarma Cave (Wolf et al., 2024) may provide one such example, with a DCF of 95%. We conclude that DCF is a valuable diagnostic tool for the identification of SAD-dominated sites and, when supporting other proxy evidence, subglacial speleothem growth.

7.6. Differentiating subglacial from other SAD systems using trace-element, paleothermometric, and biological proxy data

Our review thus far has confirmed a distinct stable-isotope signal in subglacial speleothem records and set out a theoretical framework to identify when SAD dominates the system. However, we have observed SAD is not unique to subglacial caves (e.g., Bajo et al., 2017), and non-glaciated high-Alpine caves in particular can yield similarly high $\delta^{13}C$ and low $\delta^{18}O$ values. This overlap may be explained by the aggressiveness of snowmelt and glacial runoff, which can produce a natural "acid-mine drainage" effect in periglacial and Alpine catchments where sulfide-bearing lithologies are exposed (Ilyashuk et al., 2018; Zarroca et al., 2021). Sulfide oxidation results in concomitantly low pH and high SO_4^{2-} with enhanced major cations and associated trace elements (e.g., Fe, Al, Cu, Mn, Zn, Pb) within streams as far as >10 km from the ice margin (Fortner et al., 2011; Santofimia et al., 2017; Zarroca et al., 2021). In light of this 'intermediate' phase, we propose a yet untested suite of diagnostic criteria to distinguish subglacial from periglacial and other Alpine cave settings, in addition to the first-order proxies discussed above. The principal differences between these environments are the 1) potential for soil development and other biological activity; 2) oxygen availability in surface waters; and 3) absence of a thermal buffer to prevent freezing of the karst system.

Recent studies have successfully extracted environmental DNA from speleothems in sufficient quantities for genomic sequencing (Zepeda Mendoza et al., 2016; Stahlschmidt et al., 2019), albeit with key limitations (Marchesini et al., 2022). While the absence of environmental DNA in speleothems is expected in the case of glacial cover (with the exception of cryophilic microbiota; Hodson et al., 2008), it is not exclusively indicative, due to preservation biases. Conversely, any measurable traces of surface vegetation in environmental DNA or biomarkers specific to soil-derived organic matter (Weijers et al., 2006; Kim et al., 2011) would preclude permanent ice cover. By similar reasoning, subglacial intervals of speleothem growth should be relatively depleted in trace elements associated with soil development and/or colloidal transport (e.g., Fairchild and Treble, 2009).

Subglacial speleothems should be characterized by lower $\delta^{18}O_{SO4}$ and $\Delta\delta^{18}O_{(SO4-H2O)}$ as a result of limited oxygen availability near the ice-sediment contact where sulfide oxidation occurs, relative to periglacial catchments that lack permanent ice cover (Sec. 7.4; Ilyashuk et al., 2018). Because the mean redox state of basal melt environments depends on hydraulic connectivity with the surface, we expect that speleothem $\Delta\delta^{18}O_{(SO4-H2O)}$ should progressively increase as ice thickness decreases and then as the ice margin retreats from the cave site.

The thermal dynamics of subglacial karst are difficult to assess, due to a lack of modern examples, but we can reasonably deduce that the buffering of the ice-rock interface by a warm-based glacier should result in stable cave-air T near 0 °C. Paleothermometric techniques such as the fluid-inclusion and conventional clumped-isotope (Δ_{47}) methods are sensitive to interference by disequilibrium effects, but these limitations are largely overcome with the use of a dual clumped isotope (Δ_{47}/Δ_{48}) method (Bajnai et al., 2020; Fiebig et al., 2021), which also may reduce paleo-T uncertainty. If successful, this technique could plausibly distinguish between long-term T stability in a subglacial setting, warming associated with permafrost degradation and/or glacial retreat in a periglacial catchment, and high T variability characteristics of high-elevation sites with no ice cover.

8. Conclusions

Following the pioneering work in Castleguard Cave and early conceptual models of subglacial speleothem growth, this unique archive has been developed to include more than a dozen cave sites in the European Alps. This work has yielded semi-continuous, high-resolution terrestrial records of climatic change during glacial periods in the northern mid-latitudes, which are difficult to document using conventional

paleoclimate proxies from terrestrial archives. While the mechanism and kinetics of subglacial cave systems are generally understood, there is still ample opportunity to apply a more comprehensive multiproxy approach to elucidate their geochemical behavior in relationship to glacier dynamics. Herein, we have presented a set of diagnostic criteria that can be rigorously tested against current and future subglacial speleothem collections. If successful, these datasets – already useful to interpret millennial-scale changes in regional atmospheric dynamics – may also provide vital spatiotemporal constraints on extent, thickness, and thermal properties of Pleistocene paleoglaciers.

Declaration of competing interest

The authors declare that they have no known competing financial interests or personal relationships that could have appeared to influence the work reported in this paper.

Data availability

Data will be made available on request.

Acknowledgements

CS is grateful to Augusto Mangini for his support during the first phase of research on Alpine speleothems and to Christian Stenner for discussions on Castleguard Cave. Christian Stenner and Jeremy Bruns kindly provided photographs. Peter Wynn's feedback helped to improve the chapter on sulfate proxies. Work on this review paper was partly supported by the Austrian Science Fund, grant P358770 to CS. We thank two reviewers for their constructive feedback.

References

Alexander, E.C., Dorale, J.A., Shade, B.L., Edwards, R.L., Lively, R.S., Worthington, S.R. H., Serefiddin, F., Ford, D.C., 2001. A major revision of U/Th speleothem dates from Cold Water Cave, Iowa. Geological Society of America Abstracts with programs 33 (6), 71.

Amante, C., Eakins, B.W., 2009. ETOPO1 1 Arc-Minute Global Relief Model: Procedures, Data Sources and Analysis. NOAA Technical Memorandum NESDIS. https://doi.org/10.7289/V5C8276M. NGDC-24.

Apaéstegui, J., Cruz, F.W., Vuille, M., Fohlmeister, J., Espinoza, J.C., Sifeddine, A., Strikis, N., Guyot, J.L., Ventura, R., Cheng, H., Edwards, R.L., 2018. Precipitation changes over the eastern Bolivian Andes inferred from speleothem ($\delta^{18}O$) records for the last 1400 years. Earth Planet Sci. Lett. 494, 124–134.

Arps, J., 2017. Towards ε-precision of U-series age determinations of secondary carbonates. Unpubl. PhD thesis Univ. Heidelberg.

Atkinson, T.C., 1983. Growth mechanisms of speleothems in castleguard cave, Columbia icefields, Alberta, Canada. Arctic Alpine Res. 15, 523–536.

Bajnai, D., Guo, W., Spötl, C., Coplen, T.B., Methner, K., Löffler, N., Krsnik, E., Gischler, E., Hansen, M., Henkel, D., Price, G.D., Raddatz, J., Scholz, D., Fiebig, J., 2020. Dual clumped isotope thermometry resolves kinetic biases in carbonate formation temperatures. Nature Commun. 11, 4005. https://doi.org/10.1038/s41467-020-17501-0.

Bajo, P., Borsato, A., Drysdale, R., Hua, Q., Frisia, S., Zanchetta, G., Hellstrom, J., Woodhead, J., 2017. Stalagmite carbon isotopes and dead carbon proportion (DCP) in a near-closed-system situation: an interplay between sulphuric and carbonic acid dissolution. Geochim. Cosmochim. Acta 210, 208–227.

Bajo, P., Drysdale, R.N., Woodhead, J.D., Hellstrom, J.C., Hodell, D., Ferretti, P., Voelker, A.H.L., Zanchetta, G., Rodrigues, T., Wolff, E., Tyler, J., Frisia, S., Spötl, C., Fallick, T., 2020. Persistent influence of obliquity on ice-age terminations since the Middle Pleistocene Transition. Science 367, 1235–1239.

Baker, A., Smart, P.L., Edwards, R.L., 1996. Mass spectrometric dating of flowstone from stump Cross caverns and lancaster Hole, yorkshire: palaeoclimatic implications. J. Quat. Sci. 11, 107–114.

Baker, J.L., Lachniet, M.S., Chervyatsova, O., Asmerom, Y., Polyak, V.J., 2017. Holocene warming in western continental Eurasia driven by glacial retreat and greenhouse forcing. Nat. Geosci. 10, 430–435.

Barkan, Y., Paris, G., Webb, S.M., Adkins, J.F., Halevy, I., 2020. Sulfur isotope fractionation between aqueous and carbonate-associated sulfate in abiotic calcite and aragonite. Geochim. Cosmochim. Acta 280, 317–339.

Batchelor, C.L., Margold, M., Krapp, M., Murton, D.K., Dalton, A.S., Gibbard, P.L., Stokes, C.R., Murton, J.B., Manica, A., 2019a. The configuration of Northern Hemisphere ice sheets through the Quaternary. Nat. Commun. 10, 3713. https://doi.org/10.1038/s41467-019-11601-2.

Batchelor, C.J., Orland, I.J., Marcott, S.A., Slaughter, R., Edwards, R.L., Zhang, P., Li, X., Cheng, H., 2019b. Distinct permafrost conditions across the last two glacial periods in midlatitude north America. Geophys. Res. Lett. 46, 13318–13326.

Berger, A., Loutre, M.F., 1991. Insolation values for the climate of the last 10 million years. Quat. Sci. Rev. 10, 297–317.

Berstad, I.M., Lundberg, J., Lauritzen, S.-E., Linge, H.C., 2002. Comparison of the climate during Marine Isotope Stage 9 and 11 inferred from a speleothem isotope record from Northern Norway. Quat. Res. 58, 361–371.

Bondyrev, I.V., Davitashvili, Z.V., Singh, V.P., 2015. The Geography of Georgia: Problems and Perspectives. Springer. https://doi.org/10.1007/978-3-319-05413-1.

Bonvallet, L., 2015. Evolution of the Helvetic shelf (Switzerland) during the Barremian-early Aptian: Paleoenvironmental, paleogeographic and paleoceanographic controlling factors. Unpubl. PhD thesis Univ. of Lausanne. https://core.ac.uk/download/pdf/77165502.pdf.

Borsato, A., Frisia, S., Wynn, P.M., Fairchild, I.J., Miorandi, R., 2015. Sulphate concentration in cave dripwater and speleothems: long-term trends and overview of its significance as proxy for environmental processes and climate changes. Quat. Sci. Rev. 127, 48–60.

Borsato, A., Johnston, V.E., Frisia, S., Miorandi, R., Corradini, F., 2016. Temperature and altitudinal influence on karst dripwater chemistry: implications for regional-scale palaeoclimate reconstructions from speleothems. Geochim. Cosmochim. Acta 177, 275–297.

Bottrell, S.H., 2007. Stable isotopes in aqueous sulphate as tracers of natural and contaminant sulphate sources: a reconnaissance study of the Xingwen karst aquifer, Sichuan, China. In: Parise, M., Funn, J. (Eds.), Natural and Anthropogenic Hazards in Karst Areas: Recognition, Analysis and Mitigation, vol. 279. Geological Society, London, Special Publications, pp. 123–135.

Bottrell, S.H., Tranter, M., 2002. Sulphide oxidation under partially anoxic conditions at the bed of the Haut Glacier d'Arolla, Switzerland. Hydrol. Process. 16, 2363–2368.

Bowen, G.J., Wilkinson, B., 2002. Spatial distribution of $\delta^{18}O$ in meteoric precipitation. Geology 30 (4), 315–318.

Bühler, J.C., Roesch, C., Kirschner, M., Sime, L., Holloway, M.D., Rehfeld, K., 2021. Comparison of the oxygen isotope signatures in speleothem records and iHadCM3 model simulations for the last millennium. Clim. Past 17, 985–1004.

Burns, S.J., Matter, A., Frank, N., Mangini, A., 1998. Speleothem-based paleoclimate record from northern Oman. Geology 26, 499–502.

Canfield, D.E., 2001. Biogeochemistry of Sulfur Isotopes. Reviews in Mineralogy and Geochemistry 43, 607–636.

Chen, Z., Auler, A.S., Bakalowicz, M., Drew, D., Griger, F., Hartmann, J., Jiang, G., Moosdorf, N., Richts, A., Stevanovic, Z., Veni, G., Goldscheider, N., 2017. The World Karst Aquifer Mapping project: concept, mapping procedure and map of Europe. Hydrogeol. J. 25, 771–785.

Chen, D., Feng, Q., Gong, M., 2023. Contamination characteristics and source identification of groundwater in Xishan coal mining area of Taiyuan based on hydrochemistry and sulfur–oxygen isotopes. Water 15, 1169. https://doi.org/10.3390/w15061169.

Cheng, H., Edwards, R.L., Broecker, W.S., Denton, G.H., Kong, X., Wang, Y., Zhang, R., Wang, X., 2009. Ice age terminations. Science 326, 248–252.

Cheng, H., Zhang, P.Z., Spötl, C., Edwards, R.L., Cai, Y.J., Zhang, D.Z., Sang, W.C., Tan, M., An, Z.S., 2012. The climatic cyclicity in semiarid arid central Asia over the past 500,000 years. Geophys. Res. Lett. 39, L01705 https://doi.org/10.1029/2011GL050202.

Cheng, H., Spötl, C., Breitenbach, S.F.M., Sinha, A., Wassenburg, J.A., Jochum, K.P., Scholz, D., Li, X., Yi, L., Peng, Y., Lv, Y., Zhang, P., Votintseva, A., Loginov, V., Ning, Y., Kathayat, G., Edwards, R.L., 2016. Climate variations of Central Asia on orbital to millennial timescales. Sci. Rep. 6, 36975 https://doi.org/10.1038/srep36975.

Cliff, R.A., Spötl, C., Mangini, A., 2010. U-Pb dating of speleothems from Spannagel Cave, Austrian Alps: a high resolution comparison with U-series ages. Quat. Geochronol. 5, 452–458.

Columbu, A., Sauro, F., Lundberg, J., Drysdale, R., De Waele, J., 2018. Palaeoenvironmental changes recorded by speleothems of the southern Alps (Piani Eterni, Belluno, Italy) during four interglacial to glacial climate transitions. Quat. Sci. Rev. 197, 319–335.

Comas-Bru, L., Rehfeld, K., Roesch, C., Amirnezhad-Mozhdehi, S., Harrison, S.P., Atsawawaranunt, K., Ahmad, S.M., Ait Brahim, Y., Baker, A., Bosomworth, M., Breitenbach, S.F.M., Burstyn, Y., Columbu, A., Deininger, M., Demény, A., Dixon, B., Fohlmeister, J., Hatvani, I.G., Hu, J., Kaushal, N., Kern, Z., Labuhn, I., Lechleitner, F. A., Lorrey, A., Martrat, B., Novello, V.F., Oster, J., Pérez-Mejías, C., Scholz, D., Scroxton, N., Sinha, N., Ward, B.M., Warken, S., Zhang, H., SISAL Working Group members, 2020. SISALv2: a comprehensive speleothem isotope database with multiple age–depth models. Earth Syst. Sci. Data 12, 2579–2606.

Coplen, T.B., 2007. Calibration of the calcite–water oxygen-isotope geothermometer at Devils Hole, Nevada, a natural laboratory. Geochim. Cosmochim. Acta 71, 3948–3957.

Dehnert, A., Preusser, F., Kramers, J., Akcar, N., Kubik, P.W., Reber, R., Schlüchter, C., 2010. A multi-dating approach applied to proglacial sediments attributed to the Most Extensive Glaciation of the Swiss Alps. Boreas 39, 620–632.

Deininger, M., Fohlmeister, J., Scholz, D., Mangini, A., 2012. Isotope disequilibrium effects: the influence of evaporation and ventilation effects on the carbon and oxygen isotope composition of speleothems – a model approach. Geochim. Cosmochim. Acta 96, 57–79.

Deininger, M., Hansen, M., Fohlmeister, J., Schröder-Ritzrau, A., Burstyn, Y., Scholz, D., 2021. Are oxygen isotope fractionation factors between calcite and water derived from speleothems systematically biased due to prior calcite precipitation (PCP)? Geochim. Cosmochim. Acta 305, 212–227.

Dietzel, M., Tang, J., Leis, A., Köhler, S.J., 2009. Oxygen isotopic fractionation during inorganic calcite precipitation – Effects of temperature, precipitation rate and pH. Chem. Geol. 268, 107–115.
Dreybrodt, W., 1982. A possible mechanism for growth of calcite speleothems without participation of biogenic carbon dioxide. Earth Planet Sci. Lett. 58, 293–299.
Dreybrodt, W., 1988. Processes in Karst Systems. Springer, Berlin.
Dreybrodt, W., Scholz, D., 2011. Climatic dependence of stable carbon and oxygen isotope signals recorded in speleothems: from soil water to speleothem calcite. Geochim. Cosmochim. Acta 75, 734–752.
Drysdale, R.N., Zanchetta, G., Hellstrom, J.C., Fallick, A.E., Zhao, J.-x., 2005. Stalagmite evidence for the onset of the Last Interglacial in southern Europe at 129 ± 1 ka. Geophys. Res. Lett. 32 https://doi.org/10.1029/2005GL024658.
Drysdale, R.N., Hellstrom, J.C., Zanchetta, G., Fallick, A.E., Sánchez-Goni, M.F., Couchoud, I., McDonald, J., Maas, R., Lohmann, G., Isola, I., 2009. Evidence for obliquity forcing of glacial Termination II. Science 325, 1527–1531.
Edwards, R.L., Chen, J.H., Wasserburg, G.J., 1987. ^{238}U-^{234}U-^{230}Th-^{232}Th systematics and the precise measurement of time over the past 500,000 years. Earth Planet. Sci. Lett. 81, 175–192.
Ehlers, J., Gibbard, P.L., Hughes, P.D., 2011. Quaternary glaciations - Extent and chronology. A closer look. Dev. Quat. Sci. 15, 15–28.
Fairchild, I.J., Baker, A., 2012. Speleothem Science. From Processes to Past Environments. Wiley-Blackwell, Chichester.
Fairchild, I.J., Treble, P.C., 2009. Trace elements in speleothems as recorders of environmental change. Quat. Sci. Rev. 28, 449–468.
Fairchild, I.J., L. Smith, C., Baker, A., Fuller, L., Spötl, C., Mattey, D., McDermott, F., E, I. M.F., 2006. Modification and preservation of environmental signals in speleothems. Earth Sci. Rev. 75, 105–153. https://doi.org/10.1016/j.earscirev.2005.08.003.
Fankhauser, A., McDermott, F., Fleitmann, D., 2016. Episodic speleothem deposition tracks the terrestrial impact of millennial-scale last glacial climate variability in SW Ireland. Quat. Sci. Rev. 152, 104–117.
Fiebig, J., Daëron, M., Bernecker, M., Guo, W., Schneider, G., Boch, R., Bernasconi, S.M., Jautzy, J., Dietzel, M., 2021. Calibration of the dual clumped isotope thermometer for carbonates. Geochim. Cosmochim. Acta 312, 235–256.
Fischer, A., Stocker-Waldhuber, M., Frey, M., Bohleber, P., 2022. Contemporary mass balance on a cold Eastern Alpine ice cap as a potential link to the Holocene climate. Scientifc Reports 12, 1331. https://doi.org/10.1038/s41598-021-04699-2.
Fohlmeister, J., Schröder-Ritzrau, A., Spötl, C., Frisia, S., Miorandi, R., Kromer, B., Mangini, A., 2010. The influences of hydrology on the radiogenic and stable carbon isotope composition of cave drip water, Grotta di Ernesto (Italy). Radiocarbon 52, 1529–1544. https://doi.org/10.1017/S0033822200056289.
Fohlmeister, J., Scholz, D., Kromer, B., Mangini, A., 2011. Modelling carbon isotopes of carbonates in cave drip water. Geochim. Cosmochim. Acta 75, 5219–5228. https://doi.org/10.1016/j.gca.2011.06.023.
Fohlmeister, J., Vollweiler, N., Spötl, C., Mangini, A., 2013. COMNISPA II: update of a mid-European isotope climate record, 11 ka to present. Holocene 23, 749–754.
Fohlmeister, J., Plessen, B., Dudashvili, A.S., Tjallingii, R., Wolff, C., Gafurov, A., Cheng, H., 2017. Winter precipitation changes during hte Medieval climate anomaly and the little ice age in arid central Asia. Quat. Sci. Rev. 178, 24–36.
Fohlmeister, J., Trüssel, M., Frank, N., Spötl, C., 2019. Stalagmitenwachstum der letzten 200000 Jahre in den Karsthöhlen der Melchsee-Frutt (Kerns OW). Akten des 14. Nationaler Kongress für Höhlenforschung, Sinterlaken 2019, pp. 179–184.
Fohlmeister, J., Voarintsoa, N.G., Lechleitner, F.A., Boyd, M., Brandstätter, S., Jacobson, M.J., Oster, J.L., 2020. Main controls on the stable carbon isotope composition of speleothems. Geochim. Cosmochim. Acta 279, 67–87.
Fohlmeister, J., Luetscher, M., Spötl, C., Schröder-Ritzrau, A., Schröder, B., Frank, N., Eichstädter, R., Trüssel, M., Skiba, V., Boers, N., 2023. The role of Northern Hemisphere summer insolation for millennial-scale climate variability during the penultimate glacial. Communications Earth & Environment 4, 245. https://doi.org/10.1038/s43247-023-00908-0.
Ford, D.C., Smart, C.C., 2017. Castleguard cave and karst, Columbia icefield, Alberta and British Columbia. In: Slaymaker, O. (Ed.), Landscapes and Landforms of Western Canada. Springer, Cham, pp. 227–239.
Ford, D.C., Harmon, R.S., Schwarcz, H.P., Wigley, T.M.L., Thompson, P., 1976. Geo-hydrologic and thermometric observations in the vicinity of the Columbia icefield, Alberta and British Columbia, Canada. J. Glaciol. 16, 219–230.
Fortner, S.K., Mark, B.G., McKenzie, J.M., Bury, J., Trierweiler, A., Baraer, M., Burns, P. J., Munk, L.A., 2011. Elevated stream trace and minor element concentrations in the foreland of receding tropical glaciers. Applied Geoch. 26, 1792–1801.
Frisia, S., Bini, A., Quinif, Y., 1993. Morphologic, crystallographic and isotopic study on an ancient flowstone (Grotta di Cunturines, Dolomites) - implications for paleoenvironmental reconstructions. Spéléochronos 5, 3–18.
Frisia, S., Borsato, A., Fairchild, I.J., Susini, J., 2005. Variations in atmospheric sulphate recorded in stalagmites by synchrotron micro-XRF and XANES analyses. Earth Planet Sci. Lett. 235, 729–740.
Gascoyne, M., 1992. Palaeoclimate determination from cave calcite deposits. Quat. Sci. Rev. 11, 609–632.
Gascoyne, M., Nelson, D.E., 1983. Growth mechanisms of recent speleothems from Castleguard Cave, Columbia Icefields, Alberta, Canada, inferred from a comparison of uranium-series and carbon-14 age data. Arctic Alpine Res. 15, 537–542.
Gascoyne, M., Latham, A.G., Harmon, R.S., Ford, D.C., 1983. The antiquity of Castleguard cave, Columbia icefields, Alberta, Canada. Arctic Alpine Res. 15, 463–470.
Genty, D., Baker, A., Massault, M., Proctor, C., Gilmour, M., Pons-Branchu, E., Hamelin, B., 2001. Dead carbon in stalagmites: carbonate bedrock paleodissolution vs. ageing of soil organic matter. Implications for ^{13}C variations in speleothems. Geochim. Cosmochim. Acta 65, 3443–3457. https://doi.org/10.1016/S0016-7037(01)00697-4.
Genty, D., Blamart, D., Ouahdi, R., Gilmour, M., Baker, A., Jouzel, J., Van-Exter, S., 2003. Precise dating of Dansgaard-Oeschger climate oscillations in western Europe from stalagmite data. Nature 421, 833–837.
Genty, D., Nebout, N.C., Hatté, C., Blamart, D., Ghaleb, B., Isabello, L., 2005. Rapid climatic changes of the last 90 kyr recorded on the European continent. C.R. Geoscience 337, 970–982.
Geyh, M.A., Heine, K., 2014. Several distinct wet periods since 420 ka in the Namib Desert inferred from U-series dates of speleothems. Quat. Res. 81, 381–391.
Graly, J.A., Humphrey, N.F., Licht, K.J., 2018. Two metrics describing the causes of seasonal and spatial changes in subglacial aqueous chemistry. Frontiers in Earth Science 6, 195. https://doi.org/10.3389/feart.2018.00195.
Granger, D.E., Stock, G.M., 2004. Using cave deposits as geologic tiltmeters: application to postglacial rebound of the Sierra Nevada, California. Geophys. Res. Lett. 31, L22501 https://doi.org/10.1029/2004GL021403.
Griffiths, M.L., Fohlmeister, J., Drysdale, R.N., Hua, Q., Johnson, K.R., Hellstrom, J.C., Gagan, M.K., Zhao, J.-x., 2012. Hydrological control on the dead-carbon content of a Holocene tropical speleothem. Quat. Geochronol. 14, 81–93. https://doi.org/10.1016/j.quageo.2012.04.001.
Guo, W., Zhou, C., 2019. Patterns and controls of disequilibrium isotope effects in speleothems: insights from an isotope-enabled diffusion-reaction model and implications for quantitative thermometry. Geochim. Cosmochim. Acta 267, 196–226.
Haeberli, W., Frauenfelder, R., Kääb, A., Wagner, S., 2004. Characteristics and potential climatic significance of "miniature ice caps'' (crest- and cornice-type low-altitude ice archives). J. Glaciol. 50, 129–136.
Hallet, B., 1976. Deposits formed by subglacial precipitation of $CaCO_3$. Geol. Soc. Am. Bull. 87, 1003–1015.
Hansen, M., Scholz, D., Schöne, B.R., Spötl, C., 2019. Simulating speleothem growth in the laboratory: determination of stable isotope fractionation (δ^{13}C and δ^{18}O) between H_2O, DIC and $CaCO_3$. Chem. Geol. 509, 20–44.
Harmon, R.S., Ford, D.C., Schwarcz, H.P., 1977. Interglacial chronology of the Rocky and Mackenzie Mountains based upon ^{230}Th-^{234}U dating of calcite speleothems. Can. J. Earth Sci. 14, 2543–2552.
Harmon, R.S., Schwarcz, H.P., Ford, D.C., Koch, D.L., 1979. An isotopic paleotemperature record for late Wisconsinan time in northeast Iowa. Geology 7, 430–433.
Harmon, R.S., Atkinson, T.C., Atkinson, J.L., 1983. The mineralogy of Castleguard cave, Columbia icefields, Alberta, Canada. Arctic Alpine Res. 15, 503–516.
Harris, R., Graham, K., Lavigne, J., Crisp, T., Stenner, C., 2021. Exploration, science and film project: return to Castleguard. The Canadian Caver 89, 14–24.
Häuselmann, P., Lauritzen, S.-E., Jeannin, P.-Y., Monbaron, M., 2008. Glacier advances during the last 400 ka as evidenced in St. Beatus Caves (BE, Switzerland). Quat. Int. 189, 173–189.
Häuselmann, A.D., Fleitmann, D., Cheng, H., Tabersky, D., Günter, D., Edwards, R.L., 2015. Timing and nature of the penultimate deglaciation in a high alpine stalagmite from Switzerland. Quat. Sci. Rev. 126, 264–275.
Hendy, C.H., 1971. The isotopic geochemistry of speleothems – I. The calculation of the effects of different modes of formation on the isotopic composition of speleothems and their applicability as palaeoclimatic indicators. Geochim. Cosmochim. Acta 35, 801–824.
Hill, C., Forti, P., 1997. Cave Minerals of the World, second ed. Huntsville (National Speleological Society).
Hodson, A., Anesio, A.M., Tranter, M., Fountain, A., Osborn, M., Priscu, J., Laybourn-Parry, J., Sattler, B., 2008. Glacial ecosystems. Ecol. Monogr. 78, 41–67. https://doi.org/10.1890/07-0187.1.
Holzkämper, S., Mangini, A., Spötl, C., Mudelsee, M., 2004. Timing and progression of the Last Interglacial derived from a high Alpine stalagmite. Geophys. Res. Lett. 31, L07201 https://doi.org/10.1029/2003GL019112.
Holzkämper, S., Spötl, C., Mangini, A., 2005. High-precision constraints on timing of Alpine warm periods during the middle to late Pleistocene using speleothem growth periods. Earth Planet Sci. Lett. 236, 751–764.
Honiat, C., 2018. Toward a Reconstruction of the Riss Glaciation from Sieben Hengste Cave System Stalagmites in Switzerland. Unpublished MS thesis Univ. of Innsbruck and Université Claude Bernard Lyon, 1.
Horne, G., 2017. Fifty years of exploration – Castleguard still has many unanswered questions. The Canadian Caver 86, 15–17.
Horne, G., Graham, K., Critchley, D., 2019. Use of time-lapse photography to monitor seasonal ice formation in Castleguard cave, Alberta, Canada. In: 2019 National Cave and Karst Management Symposium Proceedings, 7-11 October 2019, Bristol, Virginia. National Speleological Society, Huntsville, Alabama, USA, pp. 102–113. In: https://nckms.org/wp-content/uploads/2020/10/2019NCKMSProceedings.pdf.
Ilyashuk, B.P., Ilyashuk, E.A., Psenner, R., Tessadri, R., Koinig, K.A., 2018. Rock glaciers in crystalline catchments: hidden permafrost-related threats to alpine headwater lakes. Global Change Biol. 24, 1548–1562.
Jaillet, S., Honiat, C., Pons-Branchu, E., Couchoud, I., Hobléa, F., Racine, T., Spötl, C., 2023. Cave sediments in the western bauges karst: a record of middle and upper Pleistocene glacial advances in the French Alps. Geomorphology 433, 108707. https://doi.org/10.1016/j.geomorph.2023.108707.
Jouvet, G., Cohen, D., Russo, E., Buzan, J., Raible, C.C., Haeberli, W., Kamleitner, S., Ivy-Ochs, S., Imhof, M.A., Becker, J.K., Landgraf, A., Fischer, U.H., 2023. Coupled climate-glacier modelling of the last glaciation in the Alps. J. Glaciol. https://doi.org/10.1017/jog.2023.74.
Kim, J.-H., Talbot, H.M., Zarzycka, B., Bauersachs, T., Wagner, T., 2011. Occurrence and abundance of soil-specific bacterial membrane lipid markers in the Têt watershed

(southern France): Soil-specific BHPs and branched GDGTs. Geochemistry, Geophysics, Geosystems 12, doi.org/10.1029/2010GC003364.
Kolesar, P.T., Riggs, A.C., 2004. Influence of depositional environment on Devils Hole calcite morphology and petrology. In: Sasowsky, I.D., Mylroie, J. (Eds.), Studies of Cave Sediments. Physical and Chemical Records of Paleoclimate. Kluwer, New York, pp. 227–241.
Lauritzen, S.-E., 1995. High-resolution paleotemperature proxy record for interglaciation based on Norwegian speleothems. Quat. Res. 43, 133–146.
Lauritzen, S.-E., Skoglund, R.O., 2022. Glacier ice-contact speleogenesis in marble stripe karst. In: Shroder, J., Frumkin, A. (Eds.), Treatise on Geomorphology, second ed. Academic Press, San Diego, CA, pp. 581–615. vol. 4, Karst Geomorphology.
Lechleitner, F.A., Fohlmeister, J., McIntyre, C., Baldini, L.M., Jamieson, R.A., Hercman, H., Gąsiorowski, M., Pawlak, J., Stefaniak, K., Socha, P., Eglinton, T.I., Baldini, J.U.L., 2016. A novel approach for construction of radiocarbon-based chronologies for speleothems. Quat. Geochronol. 35, 54–65. https://doi.org/10.1016/j.quageo.2016.05.006.
Lesnek, A.J., Briner, J.P., Baichtal, J.F., Lyles, A.S., 2020. New constraints on the last deglaciation of the cordilleran ice sheet in coastal southeast Alaska. Quat. Res. 96, 140–160.
Leutz, K., 2014. Sauerstoffisotopische und mineralogische Untersuchungen an Stalagmit M39_764/1- ein Paläoklimaarchiv für das Holozän der Zentralschweiz. Unpubl. MS thesis Univ. Heidelberg.
Li, T.Y., Baker, J.L., Wang, T., Zhang, J., Wu, Y., Li, H.C., Blyakharchuk, T., Yu, T.L., Shen, C.C., Cheng, H., Kong, X.G., Xie, W.L., Edwards, R.L., 2021. Early Holocene permafrost retreat in West Siberia amplified by reorganization of westerly wind systems. Communications Earth & Environment 2, 199. https://doi.org/10.1038/s43247-021-00238-z.
Lipar, M., Martín-Pérez, A., Ticar, J., Pavsek, M., Gabrovec, M., Hrvatin, M., Komac, B., Zorn, M., Zupan Hajna, N., Zhao, J.-X., Drysdale, R.N., Ferk, M., 2021. Subglacial carbonate deposits as a potential proxy for a glacier's former presence. Cryosphere 15, 17–30.
Lisiecki, L.E., Raymo, M.E., 2005. A Pliocene-Pleistocene stack of 57 globally distributed benthic $\delta^{18}O$ records. Paleoceanography 20. https://doi.org/10.1029/2004PA001071.
Luckman, B.H., Sperling, B.J.R., Osborn, G.D., 2020. The Holocene history of the Columbia icefield, Canada. Quat. Sci. Rev. 242, 106436.
Luetscher, M., Hoffmann, D., Frisia, S., Spötl, C., 2011. Holocene glacier history from alpine speleothems, Milchbach cave, Switzerland. Earth Planet Sci. Lett. 302, 95–106.
Luetscher, M., Boch, R., Sodemann, H., Spötl, C., Cheng, H., Edwards, R.L., Frisia, S., Hof, F., Müller, W., 2015. North atlantic storm track changes during the last glacial maximum recorded by alpine speleothems. Nat. Commun. 6, 6344. https://doi.org/10.1038/ncomms7344.
Luetscher, M., Moseley, G.E., Festi, D., Hof, F., Edwards, R.L., Spötl, C., 2021. A last interglacial speleothem record from the Sieben Hengste cave system (Switzerland): implications for alpine paleovegetation. Quat. Sci. Rev. 262, 106974 https://doi.org/10.1016/j.quascirev.2021.106974.
Maire, R., 1990. La haute montagne calcaire. Karstol. - Mem. 3, 1–725.
Mangini, A., Spötl, C., Verdes, P., 2005. Reconstruction of temperature in the Central Alps during the past 2000 years from a $\delta^{18}O$ stalagmite record. Earth Planet Sci. Lett. 235, 741–751.
Mangini, A., Verdes, P., Spötl, C., Scholz, D., Vollweiler, N., Kromer, B., 2007. Persistent influence of the North Atlantic hydrography on Central European winter temperature during the last 9,000 years. Geophys. Res. Lett. 34, L02704 https://doi.org/10.1029/2006GL028600.
Marchesini, A., Festi, D., Girardi, M., Micheletti, D., Vernesi, C., Luetscher, M., 2022. Ancient DNA from speleothems: opportunity or challenge? Quat. Res. 112, 180–188. https://doi.org/10.1017/qua.2022.46.
Menounos, B., Osborn, G., Clague, J.J., Luckman, B.H., 2009. Latest Pleistocene and Holocene glacier fluctuations in western Canada. Quat. Sci. Rev. 28, 2049–2074.
McDermott, F., 2004. Palaeo-climate reconstruction from stable isotope variations in speleothems: a review. Quat. Sci. Rev. 23, 901–918.
Menounos, B., Goehring, B.M., Osborn, G., Margold, M., Ward, B., Bond, J., Clarke, G.K. C., Clague, J.J., Lakeman, T., Koch, J., Caffee, M.W., Gosse, J., Stroeven, A.P., Seguinot, J., Heyman, J., 2017. Cordilleran Ice Sheet mass loss preceded climate reversals near the Pleistocene Termination. Science 358, 781–784.
Mitchell, M.J., Krouse, H.R., Mayer, B., Stam, A.C., Zhang, Y., 1998. Use of stable isotopes in evaluating sulfur biogeochemistry of forest ecosystems. In: Kendall, C., McDonnell, J.J. (Eds.), Isotope Tracers in Catchment Hydrology. Elsevier, pp. 489–518.
Monegato, G., Scardia, G., Hajdas, I., Rizzini, F., Piccin, A., 2017. The Alpine LGM in the boreal ice-sheets game. Sci. Rep. 7, 2078. https://doi.org/10.1038/s41598-017-02148-7.
Moseley, G.M., Spötl, C., Cheng, H., Min, A., Boch, R., Edwards, R.L., 2015. Termination-II interstadial/stadial climate change recorded in two stalagmites from the north European Alps. Quat. Sci. Rev. 127, 229–239.
Mühlinghaus, C., Scholz, D., Mangini, A., 2009. Modelling fractionation of stable isotopes in stalagmites. Geochim. Cosmochim. Acta 73, 7275–7289.
Nicholson, S.L., Pike, A.W.G., Hosfield, R., Roberts, N., Sahy, D., Woodhead, J., Cheng, H., Edwards, R.L., Affolter, S., Leuenberger, M., Burns, J.S., Matter, A., Fleitmann, D., 2020. Pluvial periods in Southern Arabia over the last 1.1 million-years. Quat. Sci. Rev. 229, 106112 https://doi.org/10.1016/j.quascirev.2019.106112.
Noronha, A.L., Johnson, K.R., Hu, C., Ruan, J., Southon, J.R., Ferguson, J.E., 2014. Assessing influences on speleothem dead carbon variability over the Holocene: implications for speleothem-based radiocarbon calibration. Earth Planet Sci. Lett. 394, 20–29.
Oster, J.L., Montañez, I.P., Sharp, W.D., 2009. Stalagmite records of Pleistocene and Holocene climate from the Sierra Nevada, California. Geochim. Cosmochim. Acta Suppl. 73, A978.
Oster, J.L., Montañez, I.P., Guilderson, T.P., Sharp, W.D., Banner, J.L., 2010. Modeling speleothem $\delta^{13}C$ variability in a central Sierra Nevada cave using ^{14}C and $^{87}Sr/^{86}Sr$. Geochim. Cosmochim. Acta 72, 5228–5242.
Oster, J.L., Montañez, I.P., Mertz-Kraus, R., Sharp, W.D., Stock, G.M., Spero, H.J., Tinsley, J., Zachos, J.C., 2014. Millennial-scale variations in western Sierra Nevada precipitation during the last glacial cycle MIS 4/3 transition. Quat. Res. 82, 236–248.
Owen, R., 2017. Development and Application of Speleothem-Based Proxies for Past Climate Change. University of Oxford. Unpublished PhD thesis.
Present, T.M., Adkins, J.F., Fischer, W.W., 2020. Variability in sulfur isotope records of Phanerozoic seawater sulfate. Geophys. Res. Lett. 47, e2020GL088766 https://doi.org/10.1029/2020GL088766.
Railsback, L.B., Gibbard, P., Head, M., Voarintsoa, N.R.G., Toucanne, S., 2015. An optimized scheme of lettered marine isotope substages for the last 1.0 million years, and the climatostratigraphic nature of isotope stages and substages. Quat. Sci. Rev. 111, 94–106.
Refsnider, K.A., Miller, G.H., Hillaire-Marcel, C., Fogel, M.L., Ghaleb, B., Bowden, R., 2012. Subglacial carbonates constrain basal conditions and oxygen isotopic composition of the Laurentide Ice Sheet over Arctic Canada. Geology 40, 135–138.
Reimer, P.J., Austin, W.E.N., Bard, E., Bayliss, A., Blackwell, P.G., Bronk Ramsey, C., Butzin, M., Cheng, H., Edwards, R.L., Friedrich, M., Grootes, P.M., Guilderson, T.P., Hajdas, I., Heaton, T.J., Hogg, A.G., Hughen, K.H., Kromer, B., Manning, S.W., Muscheler, R., Palmer, J.G., Pearson, C., van der Plicht, J., Reimer, R.W., Richards, D.A., Scott, E.M., Southon, J.R., Turney, C.S.M., Wacker, L., Adolphi, F., Büntgen, U., Capano, M., Fahrni, S.M., Fogtmann-Schulz, A., Friedrich, R., Köhler, P., Kudsk, S., Miyake, F., Olsen, J., Reinig, F., Sakamoto, M., Sookdeo, A., Talamo, S., 2020. The IntCal20 Northern Hemisphere radiocarbon age calibration curve (0–55 cal kBP). Radiocarbon 62, 725–757.
Rollins, J., 2004. Caves of the Canadian Rockies and Columbia Mountains. Surrey (Rocky Mountains Books).
Samborska, K., Halas, S., Bottrell, S.H., 2013. Sources and impact of sulphate on groundwaters of Triassic carbonate aquifers, Upper Silesia, Poland. J. Hydrol. 486, 136–150.
Santofimia, E., López-Pamo, E., Palomino, E.J., González-Toril, E., Aguilera, A., 2017. Acid rock drainage in Nevado Pastoruri glacier area (Huascarán National Park, Perú): hydrochemical and mineralogical characterization and associated environmental implications. Environmental Science and Pollution Research 24, 25243–25259.
Schlüchter, C., Akcar, N., Ivy-Ochs, S., 2021. The Quaternary period in Switzerland. In: Reynard, E. (Ed.), Landscapes and Landforms of Switzerland. Springer, pp. 47–69.
Scholz, D., Mühlinghaus, C., Mangini, A., 2009. Modelling $\delta^{13}C$ and $\delta^{18}O$ in the solution layer on stalagmite surfaces. Geochim. Cosmochim. Acta 73, 2592–2602.
Seemann, R., Geyh, M.A., Franke, H.W., 1997. Altersbestimmung an Sinter- und Tropfsteinformationen der Hermannshöhle. In: Hartmann, H., Hartmann, W., Mrkos, H. (Eds.), Die Hermannshöhle in Niederösterreich, Wiss. Beih. Die Höhle, vol. 50, pp. 133–145.
Seguinot, J., Ivy-Ochs, S., Jouvet, G., Huss, M., Funk, M., Preusser, F., 2018. Modelling last glacial cycle ice dynamics in the Alps. Cryosphere 12, 3265–3285.
Sinha, A., Kathayat, G., Cheng, H., Breitenbach, S.F.M., Berkelhammer, M., Mudelsee, M., Biswas, J., Edwards, R.L., 2015. Trends and oscillations in the Indian summer monsoon rainfall over the last two millennia. Nat. Commun. 6 (1), 6309. https://doi.org/10.1038/ncomms7309.
Skiba, V., Spötl, C., Trüssel, M., Schröder-Ritzrau, A., Schröder, B., Frank, N., Eichstädter, R., Tjangiligi, R., Marwan, N., Zhang, X., Fohlmeister, J., 2023a. Millennial-scale climate variability in the Northern Hemisphere influenced glacier dynamics in the Alps around 250,000 years ago. Communications Earth & Environment 4, 426. https://doi.org/10.1038/s43247-023-01083-y.
Skiba, V., Fohlmeister, J., 2023. Contemporaneously growing speleothems and their value to decipher in-cave processes – A modelling approach. Geochim. Cosmochim. Acta 348, 381–396. https://doi.org/10.1016/j.gca.2023.03.016.
Skiba, V., Jouvet, G., Marwan, N., Spötl, C., Fohlmeister, J., 2023b. Speleothem growth and stable carbon isotopes as proxies of the presence and thermodynamical state of glaciers compared to modelled glacier evolution in the Alps. Quat. Sci. Rev. 322, 108403 https://doi.org/10.1016/j.quascirev.2023.108403.
Spötl, C., Mangini, A., 2002. Stalagmite from the Austrian Alps reveals Dansgaard-Oeschger events during isotope stage 3: implications for the absolute chronology of Greenland ice cores. Earth Planet Sci. Lett. 203, 507–518.
Spötl, C., Mangini, A., 2007. Speleothems and paleoglaciers. Earth Planet Sci. Lett. 254, 323–331.
Spötl, C., Mangini, A., 2010. Paleohydrology of a high-elevation, glacier-influenced karst system in the Central Alps (Austria). Austrian Journal of Earth Sciences 103, 92–105.
Spötl, C., Mangini, A., Frank, N., Eichstädter, R., Burns, S.J., 2002. Start of the last interglacial period at 135 ka: evidence from a high alpine speleothem. Geology 30, 815–818.
Spötl, C., Burns, S.J., Frank, N., Mangini, A., Pavuza, N., 2004. Speleothems from the high-alpine Spannagel cave, zillertal Alps (Austria). In: Sasowsky, I.D., Mylroie, J. (Eds.), Studies of Cave Sediments. Physical and Chemical Records of Paleoclimate. Kluwer, Dortrecht, pp. 243–256.
Spötl, C., Mangini, A., Richards, D.A., 2006. Chronology and paleoenvironment of Marine Isotope Stage 3 from two high-elevation speleothems, Austrian Alps. Quat. Sci. Rev. 25, 1127–1136.

Spötl, C., Holzkämper, S., Mangini, A., 2007. The Last and the Penultimate Interglacial as recorded by speleothems from a climatically sensitive high-elevation cave site in the Alps. In: Sirocko, F., Claussen, M., Litt, T., Sánchez-Goñi, M.F. (Eds.), The Climate of Past Interglacials. Elsevier, pp. 471–491. Developments in Quaternary Science Series, 7.

Spötl, C., Scholz, D., Mangini, A., 2008. A terrestrial U/Th-dated stable isotope record of the Penultimate Interglacial. Earth Planet Sci. Lett. 276, 283–292.

Stahlschmidt, M.C., Collin, T.C., Fernandes, D.M., Bar-Oz, G., Belfer-Cohen, A., Gao, Z., Jakeli, N., Matskevich, Z., Meshveliani, T., Pritchard, J.K., McDermott, F., Pinhasi, R., 2019. Ancient mammalian and plant DNA from Late Quaternary stalagmite layers at Solkota Cave, Georgia. Sci. Rep. 6. https://doi.org/10.1038/s41598-019-43147-0.

Stock, G.M., Granger, D.E., Sasowsky, I.D., Anderson, R.S., Finkel, R.C., 2005. Comparison of U–Th, paleomagnetism, and cosmogenic burial methods for dating caves: implications for landscape evolution studies. Earth Planet. Sci. Lett. 236, 388–403.

Sun, J., Kobayashi, T., Strosnider, W.H.J., Wu, P., 2017. Stable sulfur and oxygen isotopes as geochemical tracers of sulfate in karst waters. J. Hydrol. 551, 245–252.

Szczygieł, J., Hercman, H., Hoke, G., Gasiorowski, M., Blaszczyk, M., Sobczyk, A., 2020. No valley deepening of the Tatra Mountains (Western Carpathians) during the past 300 ka. Geology 48, 1006–1011.

Taylor, B.E., Wheeler, M.C., 1994. Sulfur- and oxygen-isotope geochemistry of acid mine drainage in the Western United States. In: Alpers, C., Blowes, D.W. (Eds.), Environmental Geochemistry of Sulfide Oxidation. American Chemical Society.

Tennant, C., Menounos, B., 2013. Glacier change of the Columbia icefield, Canadian Rocky mountains, 1919–2009. J. Glaciol. 59, 671–686.

Tranter, M., Sharp, M.J., Brown, G.H., Willis, I.C., Hubbard, B.P., Nielsen, M.K., Smart, C. C., Gordon, S., Tulley, M., Lamb, H.R., 1997. Variability in the chemical composition of *in situ* subglacial meltwaters. Hydrol. Process. 11, 59–77.

Vaks, A., Gutareva, O.S., Breitenbach, S.F.M., Avirmed, E., Mason, A.J., Thomas, A.L., Osinzev, A.V., Kononov, A.M., Henderson, G.M., 2013. Speleothems reveal 500,000-year history of Siberian permafrost. Science 340, 183–186.

Vaks, A., Mason, A.J., Breitenbach, S.F.M., Kononov, A.M., Osinzev, A.V., Rosensaft, M., Borshevsky, A., Gutareva, O.S., Henderson, G.M., 2020. Palaeoclimate evidence of vulnerable permafrost during times of low sea ice. Science 577, 221–225.

Vollweiler, N., Scholz, D., Mühlinghaus, C., Mangini, A., Spötl, C., 2006. A precisely dated climate record for the last 9 kyr from high alpine stalagmites. Geophys. Res. Lett. 33, L20703 https://doi.org/10.1029/2006GL027662.

Wackerbarth, A., Scholz, D., Fohlmeister, J., Mangini, A., 2010. Modelling the $\delta^{18}O$ value of cave drip water and speleothem calcite. Earth Planet Sci. Lett. 299, 387–397.

Wang, Y.J., Cheng, H., Edwards, R.L., An, Z.S., Wu, J.Y., Shen, C.-C., Dorale, J.A., 2001. A high-resolution absolute-dated late Pleistocene monsoon record from Hulu Cave, China. Science 294, 2345–2348.

Weijers, J.W.H., Schouten, S., Spaargaren, O.C., Sinninghe Damsté, 2006. Occurrence and distribution of tetraether membrane lipids in soils: Implications for the use of the TEX_{86} proxy and the BIT index. Organic Geochemistry 37, 1680–1693.

Wendt, K.A., Li, X., Edwards, R.L., Cheng, H., Spötl, C., 2021. Precise timing of MIS 7 substages from the Austrian Alps. Clim. Past 17, 1443–1454.

Wilcox, P.S., Dorale, J.A., Baichtal, J., Spötl, C., Fowell, S.J., Edwards, R.L., Kovarik, J.L., 2019. Millennial-scale glacial climate variability in Southeastern Alaska follows Dansgaard-Oeschger cyclicity. Sci. Rep. 9, 7880. https://doi.org/10.1038/s41598-019-44231-1.

Wilcox, P.S., Honiat, C., Trüssel, M., Edwards, R.L., Spötl, C., 2020. Exceptional warmth and climate instability occurred in the European Alps during the Last Interglacial period. Communications Earth & Environment 1, 57. https://doi.org/10.1038/s43247-020-00063-w.

Wildberger, A., Geyh, M.A., Henning, G., 1991. Datierungsversuche an Tropfsteinen aus dem Hölloch (Zentralschweiz). Akten des 9. nationalen Kongresses der SGH 1991, 113–119.

Winograd, I.J., Coplen, T.B., Landwehr, J.M., Riggs, A.C., Ludwig, K.R., Szabo, B.J., Kolesar, P.T., Revesz, K.M., 1992. Continuous 500,000-year climate record from vein calcite in Devils Hole, Nevada. Science 258, 255–260.

Wolf, A., Baker, J.L., Tjallingii, R., Cai, Y., Osinzev, A., Antonosyan, M., Amano, N., Johnson, K.R., Skiba, V., McCormack, J., Kwiecien, O., Chervyatsova, O.Y., Dublyansky, Y.V., Dbar, R.S., Cheng, H., Breitenbach, S.F.M., 2024. Western Caucasus regional hydroclimate controlled by cold-season temperature varaibility since the Last Glacial Maximum. Communications Earth & Environment 5, 66. https://doi.org/10.1038/s43247-023-01151-3.

Wynn, P.M., Hodson, A., Heaton, T., 2006. Chemical and isotopic switching within the subglacial environment of a High Arctic glacier. Biogeochemistry 78, 173–193.

Wynn, P.M., Fairchild, I.J., Baker, A., Baldini, J.U.L., McDermott, F., 2008. Isotopic archives of sulphate in speleothems. Geochim. Cosmochim. Acta 72, 2465–2477.

Wynn, P.M., Borsato, A., Baker, A., Frisia, S., Miorandi, R., Fairchild, I.J., 2013. Biogeochemical cycling of sulphur in karst and transfer into speleothem archives at Grotta di Ernesto, Italy. Biogeochemistry 114, 255–267.

Wynn, P.M., Fairchild, I.J., Borsato, A., Spötl, C., Hartland, A., Baker, A., Frisia, S., Baldini, J.U.L., 2018. Sulphate partitioning into calcite: experimental verification of pH control and application to seasonality in speleothems. Geochim. Cosmochim. Acta 226, 69–83.

Yonge, C.J., Krouse, H.R., 1987. The origin of sulphates in Castleguard cave, Columbia icefields, Canada. Chem. Geol. 65, 427–433.

Yukimoto, S., Adachi, Y., Hosaka, M., Sakami, T., Yoshimura, H., Hirabara, M., Tanaka, T.Y., Shindo, E., Tsujino, H., Deushi, M., Mizuta, R., Yabu, S., Obata, A., Nakano, H., Koshiro, T., Ose, T., Kitoh, A., 2012. A new global climate model of the Meteorological Research Institute: MRI-CGCM3 — model description and basic performance. Journal of the Meteorological Society of Japan. Ser. II 90, 23–64.

Žák, K., Onac, B.P., Kadebskaya, O.I., Filippi, M., Dublyansky, Y., Luetscher, M., 2018. Cryogenic mineral formation in caves. In: Perşoiu, A., Lauritzen, S.-E. (Eds.), Ice Caves. Elsevier, pp. 123–162.

Zarroca, M., Roqúe, C., Linares, R., Salminci, J.G., Gutiérrez, F., 2021. Natural acid rock drainage in alpine catchments: a side effect of climate warming. Science of the Total Environment 778, 146070. https://doi.org/10.1016/j.scitotenv.2021.146070.

Zasadni, J., 2009. Deglacjacja Alp Zillertalskich (Austria) W Późnym Glacjale I Holocenie (Deglaciation of the Zillertal Alps (Austria) in the Late Glacial and Holocene). Unpublished PhD thesis Uniwersytet Jagielloński, Kraków.

Zepeda Mendoza, M.L., Lundberg, J., Ivarsson, M., Campos, P., Nylander, J.A.A., Sallstedt, T., Dalen, L., 2016. Metagenomic analysis from the interior of a speleothem in Tjuv-Ante's Cave, northern Sweden. PLoS ONE 11 (3), e0151577. https://doi.org/10.1371/journal.pone.0151577.